RSC Advances

ROYAL SOCIETY OF CHEMISTRY

www.rsc.org/advances

Manuscript ID RA-ART-09-2014-010324 (Revised)

Ligand Substitution and Electron Transfer Reactions of *trans*-(diaqua)(salen)manganese(III) with oxalate: an experimental and computational Study

Akshaya K. Kar[a], Achyut N. Acharya[b], V. Rao Mundlapati[c], Guru C. Pradhan[a], Himansu S. Biswal*[c] and Anadi C. Dash*[a]

[a] Department of Chemistry Utkal university, Bhubaneswar 751004, India

[b] Department of Chemistry, College of Engineering and Technology, Bhubaneswar 751003, India

[c] School of Chemical Sciences, National Institute of Science Education and Research (NISER), Institute of Physics Campus, Bhubaneswar 751 005, India

Corresponding authors e-mail IDs: acdash41@gmail.com, himansu@niser.ac.in

Abstract. The *trans*-$Mn^{III}(salen)(OH_2)_2^+$ undergoes reversible aqua ligand substitution by HOX^- (H_2salen = *N,N′*- bis(salicylidene)ethane-1,2-diamine; HOX^- = $^-O\text{-}COCO_2H$) with $k_1/dm^3\ mol^{-1}\ s^{-1}$ (k_{-1}/s^{-1}) = 11.8 ± 0.7 (0.255 ± 0.02), $\Delta H^{\neq}$/ kJ mol^{-1} = 54.6 ± 0.8 (64.2 ± 6.7), $\Delta S^{\neq}$/ J K^{-1} mol^{-1} = – 41.2 ± 2.6 (–40.8 ± 22.7) at 25.0°C and $\boldsymbol{I}$ = 0.3 mol dm^{-3}. The low values of the activation enthalpy and nearly the same and negative values of the activation entropy are ascribed to an associative transition state for this interchange process ($\boldsymbol{I}_a$ mechanism). The redox reaction that follows involves several paths and the products are Mn^{II} and CO_2 identified by ESR spectroscopy and conventional test respectively. The rate retardation by acrylamide monomer with no perceptible polymerization during the course of the redox reaction supports the involvement of the radical intermediate, $C_2O_4^{-\cdot}$ (= CO_2+$CO_2^{-\cdot}$) which succeeds in reducing Mn^{III} species much faster than the dimerisation of its congener, $CO_2^{-\cdot}$ in keeping with the stoichiometry,|[ΔMn^{III}]/[OX]$_T$| = 2 . The *trans*-[Mn^{III}(salen)(OH_2)(HOX)

and its conjugate base, *trans*-Mn^{III}(salen)$(OH_2)(OX)^-$ are virtually inert to intra molecular reduction of Mn^{III} centre by the bound oxalate species but undergo facile electron transfer by H_2OX, HOX^- and very slowly by OX^{2-} following the reactivity sequence, $k_{H2OX} > k_{HOX} >>> k_{OX}$ and featuring second order kinetics. The rate retardation by the anionic micelles of SDS (sodium dodecyl sulfate) and rate enhancement by N_3^- provide supportive evidences in favor of the proposed mechanistic pathways. The structure optimization of *trans*-Mn^{III}(salen)(OH_2)(HOX) **(A)**, *trans*-Mn^{III}(salen)$(HOX)_2^-$ **(B)**, *trans*-Mn^{III}(salen)$(OH_2)(OX)^-$ (**C**), *trans*-Mn^{III}(salen)$(OH_2)(H_2OX)^+$(**E_1**), and trans-Mn^{III}(salen)(HOX)(H_2OX) **(E_2)** {all high spin $Mn^{III}(d^4)$} by Density Functional Theory (**DFT**) reveals that the structural *trans*-effect of the unidentately bonded OX^{2-} in **C** is the strongest and Mn^{III} assumes five coordination with the H_2O molecule (displaced from the Mn^{III} centre) hydrogen bonded to the phenoxide oxygen moiety. The computational study highlights different modes of H-bonding in structures A-E. The activation parameters for the redox reactions, A + HOX^- and A + H_2OX, $\Delta H^{\neq}$/kJ mol^{-1}($\Delta S^{\neq}$/J K^{-1} mol^{-1}): 42.5 ± 6.2, (–106 ± 20) and 71.7 ± 7.7 (+12 ± 25) respectively are indicative of different degrees of ordering and reorganization of bonds as expected in the case of proton coupled electron transfer (PCET) process.

Keywords. Oxalate, Mn^{III}(salen), Kinetics, Electron transfer, DFT.

Running head line : *Reactions of trans-(diaqua)(salen)manganese(III) with oxalate*

A table of Contents entry

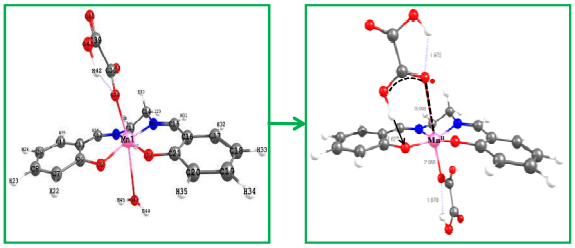

Mn^{III}(salen)$(OH_2)_2^+$ undergoes reversible anation by HOX^- via $\boldsymbol{I}_a$ mechanism followed by proton controlled electron transfer involving Mn^{III}(salen)(HOX) and H_2OX.

1. Introduction

Mn^{III} complexes with salen (H_2salen= *N,N′*- bis(salicylidene)ethane-1,2-diamine) motif are models for catalase and superoxide dismutase (SOD) activities.[1-4] Many intricate diseases like, Alzheimer, cancer, multiple sclerosis, heart and brain stokes are supposed to be related to the superoxide activity and Mn^{III}(salen) complexes have been shown as promising therapeutics.[1,3,5] The interaction of bioactive ROS (Reactive Oxygen Species) with the Mn^{III} centre of Mn^{III}(salen) moiety is a primary feature in such processes. Mn^{III}(salen) complexes have been used as catalysts in the epoxidation of olefins, and other organic transformations.[6-9] A review on the redox reactions of mononuclear Mn^{III} complexes, essentially of aminopolycarboxylate ligands, have appeared several years ago which describes briefly the mechanistic aspects of such reactions.[10] Nature's water oxidation catalyst (WOC) responsible for photo-catalyzed O_2 evolution from water is a tetra manganese cluster with Mn^{III}-Mn^{IV} coupled system which is believed to undergo redox cycling of the oxidation states of the Mn centres.[11-13] Recent investigations on the oxidation of oxalate, an ubiquitous moiety in biological domain, by oxalate oxidase have revealed the importance of Mn^{III} centre in catalyzing the oxidation of oxalate.[14,15] It involves an intermediate Mn^{III}–monooxalate complex in the monodentate form and electron transfer from the bound oxalate species to Mn^{III} centre is considered to be rate limiting. Mn^{III}(salen) may be used to model this reaction. However, the studies devoted to understand the mechanisms of ligand substitution and redox reactions of Mn^{III} are limited. In view of the importance of oxalate in biology and Mn^{III}(salen) as a suitable oxidant for oxalate oxidation, we, in continuation with our investigations[16,17]of the mechanism of ligand substitution and electron transfer at Mn^{III} centre, present here a thorough study on *trans*-Mn^{III}(salen)$(OH_2)_2^+$ + oxalate system over extended pH and temperature ranges. To the best of our knowledge there is no earlier

literature report on such a study, although oxidation of oxalate by higher valent manganese has been topic of several investigations in the past.[18, 19]

2 Experimental

2.1 *Materials and reagents*

Mn^{III}(salen)Cl,H_2O was received from our earlier work and synthesized when required and purity checked by elemental analysis and UV-Vis, I. R. spectra.[17] This complex undergoes fast aquation to $Mn^{III}(salen)(OH_2)_2^+$ when dissolved in water.[16,17] The optical spectrum of the diaqua complex in aqueous medium (pH 3) displays $\lambda_{max,}$ nm (ε_{max}, dm^3 mol^{-1} cm^{-1}) : 235(40,240), 279 (18,120) which agreed well with the previously reported values.[17] The G. R. grade (E. Merck) oxalic acid (H_2OX), potassium oxalate, perchloric acid, sodium hydroxide and glacial acetic acid were used as received. All other reagents were of highest grade purity available. Freshly prepared doubly distilled water received from an all glass (borosilicate) distillation set was used to prepare the solutions; the second distillation of water was made through alkaline $KMnO_4$. $NaClO_4$ used for ionic strength adjustment was prepared by mixing requisite amounts of the standardized solutions of NaOH and $HClO_4$. Stock solution of $NaClO_4$ (1 mol dm^{-3}) was prepared from time to time and adjusted to pH 6 and the concentration checked by a combined ion-exchange alkalimetric procedure using Dowex 50W X8 resin in the H^+ form. The stock solution of the complex (5 x 10^{-3} mol dm^{-3}, pH ~ 5) was protected from light and stored in a refrigerator at ~20°C when not in use. It was not allowed to age for more than 24 hrs.

2.2 *Physical measurements*

A Perkin Elmer Lambda25 and a Systronics (India) model 118 UV-visible spectrophotometers with a matched pair of 10mm quartz cells were used for all absorbance

measurements. The I. R. measurements were made on a Perkin Elmer FTIR spectrometer, model Spectrum2 using KBr pellet. Fluorescence measurements were made on a JASCO spectrofluorimeter model FP – 8200 using Xe/D_2 light sources; band width was set at 10nm and scan speed was 100nm/min. The excitation wavelength (λ_{exct}) was set at 265 nm and spectral scans covered 340 – 500nm. The intensity of emission at any wavelength was normalized as $\boldsymbol{I}_\lambda/\boldsymbol{I}^W{}_\lambda max$ where $\boldsymbol{I}^W{}_\lambda max$ denotes intensity at the wavelength maximum in absence of SDS. The ESR measurement was performed on a JEOL (Japan) JES-FA 200 ESR spectrometer at room temperature operating in X-band mode (8.75-9.65 GHz, power 1.08W, sensitivity 7 x 10^9 spins/0.1mT, resolution 2.35 μT). The pH measurements were made with a Systronics (India) pH meter model 335 using a glass-Ag/AgCl, Cl^- (3 mol dm^{-3} NaCl) electrode CL 51. NBS buffers of pH 4.01, 6.86 and 9.20 prepared from KHphthalate, Na_2HPO_4/ KH_2PO_4, and $Na_2B_4O_7$, $10H_2O$ respectively were used to calibrate the pH meter. The measured pH of the reaction medium was converted to $p[H^+]$ (= $-\log[H^+]$) established by a calibration curve using dilute $HClO_4$ solutions ($1.98 \times 10^{-2} \leq [H^+]/ \text{mol dm}^{-3} \leq 1.00 \times 10^{-5}$) at the same ionic strength as maintained in the reaction media ($\boldsymbol{I}$ = 0.3 mol dm^{-3}).[20]

2.3 *Kinetics*

The fast kinetics measurements were performed on a KinetAsyst SF-61 SX2 single mixing stopped flow spectrophotometer; the data acquisition and analysis was made using kinetic studio software version 0.94, application version 1.12 (TGK Scientific, U. K). The flow module and the mixing chamber were thermostatted to the desired temperature by circulating water from a refrigerated/heating water bath (Julabo F12-ED). One of the syringes was loaded with the solution of *trans*- $Mn^{III}(salen)(OH_2)_2^+$ complex (*in situ* generated) while the other contained the desired mixture of oxalic acid, $HClO_4$ and $NaClO_4$ such that after mixing the final ionic strength was set at 0.3 mol dm^{-3}. The available pK values of oxalic acid (see later) were used to calculate the ionic composition so as to set the ionic strength at the desired

value. Rate measurements were made at 380 nm under pseudo-first order conditions. The absorbance versus time plots were biphasic over extended time scale (see Figures S1(a, b)) thus indicating the rapid formation of an intermediate followed by its decay at long time scale. The two processes were treated independently. The initial fast rise of absorbance with time was fitted to equation (1) to get k_{obs}^{f} and $\boldsymbol{A}_{eq}$. Data fitting using the software package (see above) for any individual run was within ± 1%. At least 6-10 measurements were made for each run and k_{obs}^{f} could be reproduced within ± 5% ($\sigma_{(k_{obs}^{f})}/k_{obs}^{f} \leq \pm 0.05$).

$$\boldsymbol{A}_t = \boldsymbol{C}_1 \exp(-k_{obs}^{f} t) + \boldsymbol{A}_{eq} \qquad (1)$$

The values of A_{eq} were dependent on $[OX]_T$ for a given $[H^+]$ and $[complex]_T$ indicating that the formation of the intermediate was equilibrium controlled. A limited number of runs for the slow phase were made by stopped flow spectrophotometry wherever possible. The absorbance – time data for the slow phase of the reaction also studied under pseudo-first order conditions fitted to a single exponential equation with $\boldsymbol{A}_\infty$ close to zero ($\boldsymbol{A}_t = \boldsymbol{C}_2 \exp(-k_{obs}^{s} t) + \boldsymbol{A}_\infty$) and the corresponding rate constants (k_{obs}^{s}) were calculated. Most rate measurements for the slow reactions were conveniently made by batch sampling technique at 25.0 - 40.0 ^{o}C.[17] The concentration of the complex, $[Mn^{III}(salen)(OH_2)_2^{+}]$ was varied as (0.6-1.22) x 10^{-4} mol dm^{-3} and that of $[OX]_T$ (= total oxalic acid concentration) in the range 0.0005- 0.1 mol dm^{-3}. The ionic strength of the medium was fixed at 0.3 mol dm^{-3} ($NaClO_4$) unless otherwise quoted. The pH of the reaction mixtures was varied by self buffering due to H_2OX /HOX^- and HOX^-/OX^{2-}. The observed rate constants (k_{obs}^{s}) were calculated by fitting the absorbance (A_t) – time (t) data to a single exponential equation as mentioned above. A_∞ was close to zero for the completion of the reaction which was further verified by simulating the reaction mixture at complete reaction with appropriate solutions made out of Mn^{II} acetate, oxalic acid and other components at the same pH (for this the medium was 5% MeOH-water v/v as H_2salen was prepared in MeOH). The initial absorbance was in the range 0.4-0.6. For

very slow reactions ($k_{obs}^{s} \sim 10^{-5} - 10^{-6}$ s^{-1}) the rate constants were evaluated by the method of initial rate as described earlier.[17] $\sigma(k_{obs}^{s})/k_{obs}^{s}$ was generally better than ± 2% while the same from the initial rate method was ~ ± 6%.

2.4 *Initial fast reaction*

The initial fast reaction was considered to be the reversible complexation of $Mn^{III}(salen)(OH_2)_2^{+}$ with oxalate species. The k_{obs}^{f} values at 20 - 40°C are collected in Table S1(a). In the medium comprising $HClO_4$ and oxalic acid (see Table S1(a)), $[OX]_T$ is partitioned between H_2OX and HOX^- (pK_1 = 1.00 – 1.03, pK_2 = 3.59–3.64 for H_2OX at 20 - 40°C, I = 0.3 mol dm^{-3} see Table S1(b)).[21]

$$H_2OX \underset{}{\overset{K_1}{\rightleftharpoons}} H^+ + HOX^- \overset{K_2}{\rightleftharpoons} H^+ + OX^{2-} \qquad (2)$$

However, the concentrations of different oxalate species may be expressed as $[HOX^-] = f_1[OX]_T$, $[H_2OX] = f_2[OX]_T$, and $[OX^{2-}] = f_3[OX]_T$ where $f_1 = K_1[H^+]/D$, $f_2 = [H^+]^2/D$, $f_3 = K_1K_2/D$ and $D = [H^+]^2 + K_1[H^+] + K_1K_2$. The values of $[H^+]$, $[HOX^-]$ and $[H_2OX]$ were computed from the initial analytical values of $[HClO_4]$ and $[OX]_T$ considering the first stage acid dissociation of H_2OX : $[H^+] = [HClO_4] + X$, X (= $[HOX^-]$) being the acceptable solution of Eq. (3), and $[H_2OX] = [OX]_T - X$.

$$X^2 + ([HClO_4] + K_1) - K_1[OX]_T = 0 \qquad (3).$$

The k_{obs}^{f} data were fitted to Eq. (4) valid for Scheme 1 by a least squares computer program.

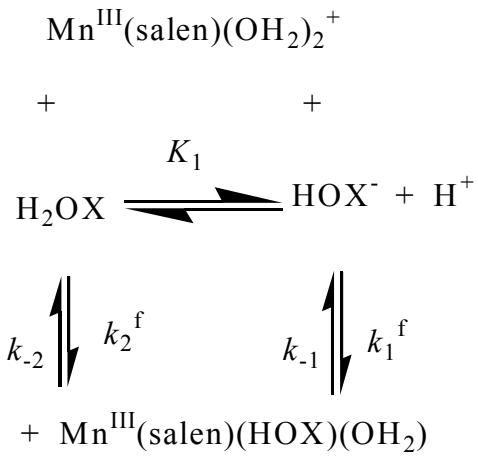

Scheme 1- Complexation of *trans*-$Mn^{III}(salen)(OH_2)_2^+$ by HOX^-/H_2OX

$$k_{obs}^{f} = (k_1^{f} f_1 + k_2^{f} f_2)([OX]_T + Q_1^{-1}/f_1) \quad (4)$$

In Eq. (4) Q_1 denotes the equilibrium constant for the formation of $Mn^{III}(salen)(HOX)(OH_2)$ (Eq. 5)

$$Q_1 = [Mn^{III}(salen)(HOX)(OH_2)]_{eq} / [Mn^{III}(salen)(OH_2)_2^+]_{eq}\,[HOX^-]_{eq} \quad (5),$$

f_1 and f_2 are the fractions of $[OX]_T$ as HOX^- and H_2OX , and k_1^{f} and k_2^{f} are the second order rate constants for the formation of $Mn^{III}(salen)(OH_2)(HOX)$ by HOX^- and H_2OX (see Scheme 1) respectively. The calculated rate, equilibrium and activation parameters are collected in Table S1(c).

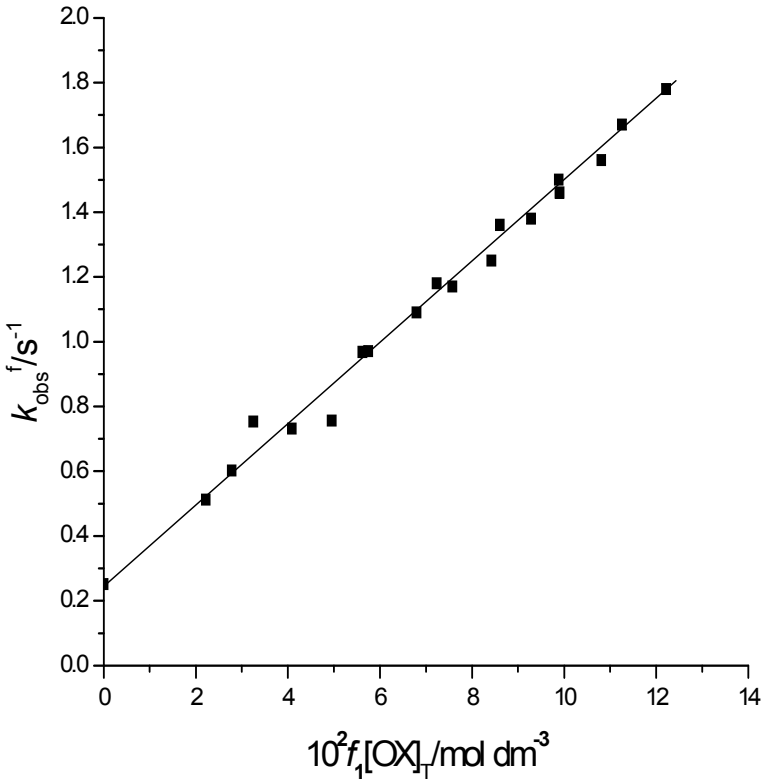

171

172 Figure 1- Formation of $[Mn^{III}(Salen)(OH_2)(HOX)]$ .k_{obs}^{f} / s^{-1} vs. $10^2 f_1[OX]_T$/ mol dm^{-3}

173 plot at 25°C.

174

175 Table 1- Comparison of the rate and activation parameters for the formation/dissociation of

176 some Mn^{III} complexes.

Reaction : R = Mn^{III}(salen)	k^a (30°C)	$\Delta H^{\neq}$/ kJ mol^{-1}	$\Delta S^{\neq}$/ J K^{-1} mol^{-1}	Ref.
$R(OH_2)_2^+ + HOX^- \rightarrow Mn^{III}(salen)(OH_2)(HOX)$	17.5 ± 1.1	54.6 ± 0.8	-41.2 ± 2.6	*b*
$R(OH_2)(HOX) \rightarrow Mn^{III}(salen)(OH_2)_2^+ + HOX^-$	0.47 ± 0.07	64.2 ± 6.7	-40.8 ± 22.7	*b*
$R(OH_2)_2^+ + HSO_3^- \rightarrow Mn^{III}(salen)(OH_2)(HSO_3)$	(3.0 ± 0.3) x 10^2	42.4 ± 0.2	–55.3 ± 0.6	*c*
$R(OH_2)_2^+ + SO_3^{2-} \rightarrow Mn^{III}(salen)(OH_2)(SO_3)^-$	(1.10 ± 0.08) x 10^3	33.0 ± 3.0	–75 ± 10	*c*
$R(OH_2)(OH) + SO_3^{2-} \rightarrow R(OH)(SO_3)^{2-}$	(2.1 ± 0.2) x 10^3	32.4 ± 0.3	–72.9 ± 0.6	*c*

$R(OH_2)(OH) + H_2Q \rightarrow R(OH)(H_2Q)$	21.8 ± 0.5			*d*
$R(OH_2)(OH) + HQ^- \rightarrow R(OH)(HQ)^-$	(1.4± 0.2) x 10^3			*d*
$R(OH_2)(OH) + H_2Cat \rightarrow R(OH)(H_2Cat)$	1.91 ± 0.41			*d*
$R(OH_2)(OH) + HCat^- \rightarrow R(OH)(HCat)^-$	(2.2 ± 0.3) x 10^2			*d*
$R(OH_2)_2^+ + H_2Asc \rightarrow R(OH_2)(H_2Asc)^+$	1.2	72.6	+ 2.5	e
$Mn^{III}(EDTA)(OH_2)^- + N_3^- \rightarrow Mn^{III}(EDTA)(N_3)^{2-}$	0.16	57.4 ± 0.9	– 71.3 ± 2.9	f
$Mn^{III}(EDTA)(N_3)^{2-} \rightarrow Mn^{III}(EDTA)(OH_2)^- + N_3^-$	4.7 x 10^{-3}	54.4 ± 0.7	–110 ± 3	f

[a] units : $dm^3\ mol^{-1}\ s^{-1}$ (s^{-1}) for the formation (dissociation) reactions. ***I*** = 0.3 mol dm^{-3}.

[b] this work. [c]ref. 16. [d] ***I*** = 0.2 mol dm^{-3}; hydroquinone (H_2Q) and catechol (H_2Cat) (ref. 22).

[e] 28°C; ascorbic acid (H_2Asc) (ref. 33). [f] ***I*** = 0.25 mol dm^{-3}(ref. 36).

It turns out that $k_2^f f_2$ term is statistically insignificant at all temperatures. Thus neglecting $k_2^f f_2$ term and setting $k_1^f Q_1^{-1} = k_{-1}^f$ Eq. (4) can be rearranged to Eq. (6).

$$k_{obs}^f = k_1^f f_1 [OX]_T + k_{-1}^f \quad (6)$$

A representative plot at 25°C (see Figure 1) bears this fact. As a check the equilibrium absorbance data (A_e) from the stopped flow runs for a constant $[complex]_T$ but varying $[OX]_T$ and $[H^+]$ (see Table S1a) are used to calculate Q_1 from the linear plots of $1/(A_e - A_0)$ versus $1/(f_1[OX]_T)$ (see Eq.7); here A_0 and A_c denote the absorbances of $Mn^{III}(salen)(OH_2)_2^+$ and $Mn^{III}(salen)(HOX)(OH_2)$ respectively at the same total concentration of the complex.

$$1/(A_e - A_0) = 1/[Q_1(A_c - A_0)\ x\ f_1[OX]_T] + 1/(A_c - A_0) \quad (7).$$

The calculated values of Q_1 are 40.1± 2.0, 42.6 ± 1.0, 41.2 ± 2.3 and 40.6 ± 2.7 $dm^3\ mol^{-1}$ at 20.0°, 25.0°, 30.0° and 40.0°C respectively which compare well with the values obtained from the kinetic data (see Table S1c, foot note *a*). As Q_1 shows little variation with

temperature its mean value from kinetic and equilibrium measurements (Q_1 = 42.0 ± 0.7 dm^3 mol^{-1} at 20 – 40°C) is used for all other calculations. A comparison of the rate and activation parameters for the reversible formation of some Mn^{III} complexes is made in Table 1.

2.5 *Redox reaction*

2.5.1 Product identification and stoichiometry

The time dependent spectral scans of the reaction mixture containing Mn^{III} complex and oxalic acid at pH = 4.17 is presented in Figure S2. Similar trend is observed at pH = 1.44.

The maxima around 285 and 390 nm (broad) characteristics of the parent complex is lost during the course of the reaction with the development of a maximum at 325 nm(broad). This is in good agreement with the spectrum of the mixture of Mn^{II} acetate + salen + H_2OX at the same pH and respective concentrations of the reactants, left to equilibration (see experimental section). The maximum at 325nm is, however, considerably reduced in intensity at lower pH. Acetate ion/acetic acid at low concentration (~(1.2–2.4) x 10^{-4} mol dm^{-3}) originating from $Mn(OAc)_2$ has no effect. The broad 325 nm peak is attributed to $Mn^{II}(salen)(OH_2)(OX/OXH)^{2-/-}$ in equilibrium with $Mn^{II}(salen)(OH_2)_2$. The ESR spectrum of the spent reaction mixture displayed 6 line spectrum characteristic of Mn^{II} (see Figure 2) thus establishing the Mn^{III}(salen) /oxalate redox reaction.

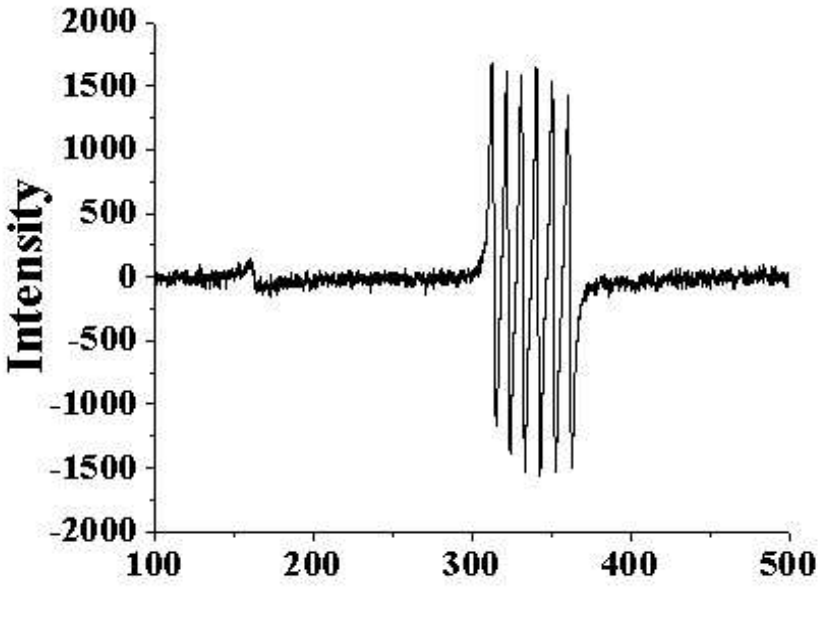

Figure 2. ESR spectrum (X-band) of the product Mn^{II} in the reduction of *trans*-$Mn^{III}(Salen)(OH_2)_2^+$ by oxalate (pH 1.8, ~ 27°C), g =1.9968. Intensity versus **H/mT** plot.

The formation of CO_2 was qualitatively established by the conventional test as follows. The reaction mixture ($[Mn^{III}(Salen)(OH_2)_2^+]_T$ = 3 x 10^{-3} and $[OX]_T$ = 0.02 mol dm^{-3}, pH = 3.5, 40°C) was set aside for $10t_{1/2}$ and then treated with a slight excess $CaCl_2$ followed by aqueous NH_3 resulting in a white precipitate. This was allowed to coagulate, collected by filtration, air dried and treated with dilute HCl when a colorless gas with effervescence (characteristic of CO_2) evolved. Our attempts to perform a quantitative analysis of the unreacted oxalate by $KMnO_4$ titration in acid medium after precipitating it as CaC_2O_4 from ammoniacal solution was unsuccessful due to the presence of the salen ligand. Based on the identified products we propose the following stoichiometry:

$$2Mn^{III}(salen)(OH_2)_2^+ + OXH^- + 3H^+ = 2Mn^{II} + 2H_2salen + 2CO_2 + 2H_2O \quad (8).$$

Similar relation can be written for H_2OX or OX^{2-}. It may be also noted that under mild acidic condition H_2salen undergoes hydrolysis to salicylaldehyde and *bis N*-protonated ethylenediamine as the final end products.

2.5.2 *Analysis of Rate data for redox reaction*

The rate data for the redox reaction are collected in Tables S2-S5. A preliminary rate measurement in absence of oxalic acid but in acid medium at $[HClO_4] \leq 0.02$ mol dm^{-3} (25-40°C) indicated that the complex is significantly inert to the acid catalyzed decomposition. This is indicated by the constancy of the molar extinction coefficient of the complex over an extended time period, $\varepsilon_{380\,nm}$ /dm^3 mol^{-1} cm^{-1} ($[HClO_4]$/ mol dm^{-3}) : 5024 ± 5(0.01), 4930 ± 8 (0.02) at 25°C for 4.63 hrs; 4970 ± 6 (0.01), 4944 ± 12 (0.01), 5123 ± 13 (0.01) at (30 - 40)°C for 4.5 hrs. However, there was a slow H^+ - catalyzed decomposition of the complex at $[H^+] \geq 0.05$ mol dm^{-3},$10^5 k_{obs}$/ s^{-1}(t/°C) ; 0.32 ± 0.05(25), 0.70 ± 0.020(30), 1.28 ± 0.05(35), and 1.85 ± 0.04(40). Hence all our measurements for redox reaction was restricted to *ca.* $[H^+] \leq 0.05$ mol dm^{-3} at which the k_{obs}^s at the lowest $[OX]_T$ (= 0.5 x 10^{-3} mol dm^{-3}) was ≥ 12 times higher than the same for the H^+- catalyzed decomposition of the complex. The correction of k_{obs}^s for the H^+-catalyzed decomposition of the complex was insignificant and hence was neglected in the analysis of the rate data.

The k_{obs}^s versus $[OX]_T$ plots at $[HClO_4]$= 0.05 mol dm^{-3} and pH = 3.10 ± 0.09 (see Figures S3(a, b)) are distinctly nonlinear. The observed trend shows greater than first-order dependence of k_{obs}^s on $[OX]_T$. Further k_{obs}^s at constant $[OX]_T$ = 0.005 mol dm^{-3} approaches a low limiting value around pH 5 (~10^{-6} s^{-1}, see Figure S3c) indicating that OX^{2-} is not an efficient reductant as HOX^- and H_2OX.

A limited number of runs at 35°C were made at $5.04 \leq pH \leq 6.72$, $0.005 \leq [OX]_T$/mol $dm^{-3} \leq 0.1$ in order to establish the redox activity of *trans*-Mn^{III}(salen))$(OH_2)(OX)^-$. Due to the solubility limitation of $Na_2C_2O_4$ the source of oxalate was $K_2C_2O_4$ and ionic strength was adjusted by KCl. The presence of chloride under the conditions had no perceptible effect on the absorption spectrum of the di-aqua complex discounting its interference. Under this

condition $[OX]_T = [HOX^-] + [OX^{2-}]$ and the diaqua Mn^{III} complex predominates (~80%). Here again a nonlinear and greater than first order dependence of k_{obs}^s with $[OX]_T$ at constant pH (= 5.27 ± 0.07) was observed (Figure S3d). Considering these facts Scheme 2 is proposed for the overall reaction for which k_{obs}^s (without considering the reaction stoichiometry; k_{icorr} = $k_i/2$, i = 0 – 7) is given by Eq. (9),

$$k_{obs}^s = \frac{k_0Q_1f_1[OX]_T + k_1Q_1(f_1[OX]_T)^2 + k_2Q_1f_1f_2[OX]_T^2 + k_3f_2[OX]_T + k_4Q_2f_3[OX]_T + k'f_1f_3[OX]_T^2 + k_6Q_2(f_3[OX]_T)^2}{1 + K_M/[H^+] + Q_1f_1[OX]_T(1 + K_2'/[H^+])} \quad (9)$$

where f_is (i = 1 - 3) are as defined earlier, $k' = k_5Q_2 + k_7Q_1$, and k_is (i = 0 - 7), Q_1, Q_2 (= Q_1K_2'/K_2) and K_2' are the rate and equilibrium parameters respectively (see Scheme 2). The k_{obs}^s data at 1.26 ≤ pH ≤ 5.08 and low $[OX]_T$ (see Tables S2-S4) could be satisfactorily analyzed by Eq.(10) a limiting form of Equation (9), as detailed below.

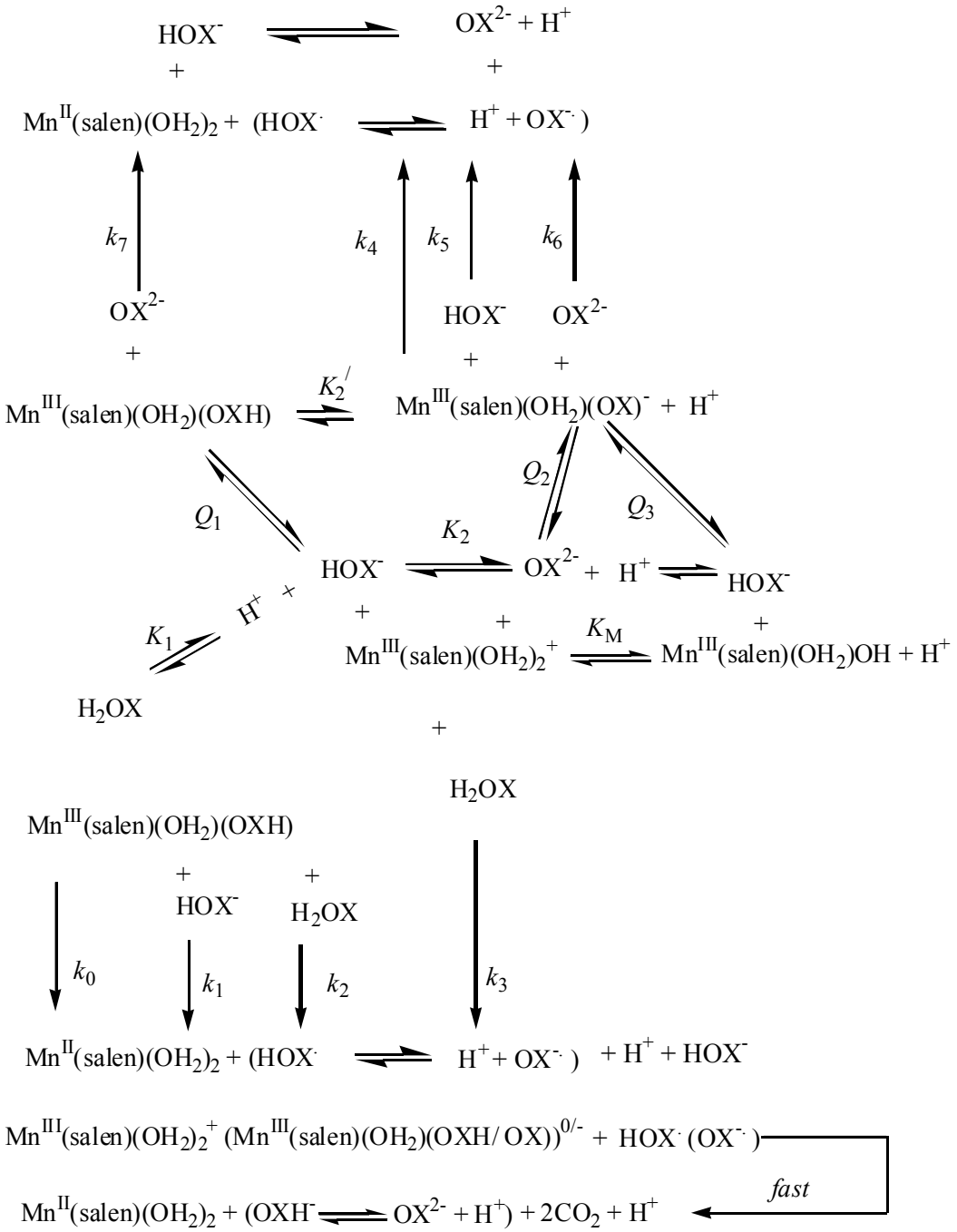

261

262 Scheme 2- Reduction of *trans*-$Mn^{III}(salen)(OH_2)_2^+$ by Oxalate.

$$k_{obs}{}^{s} = \frac{k_0 Q_1 f_1 [OX]_T + k_1 Q_1 (f_1 [OX]_T{}^2 + k_2 Q_1 f_1 f_2 [OX]_T{}^2 + k_3 f_3 [OX]_T}{1 + Q_1 f_1 [OX]_T (1 + K_2^{/}/[H^+])} \quad (10)$$

263
264

The species, H_2OX, will not exist in significant concentrations under the pH conditions $2.9 \leq pH \leq 5.08$. This amounts to a reasonable choice of neglecting the k_2 and k_3 terms of equation (10) to treat the k_{obs}^{s} data at low $[OX]_T$. On this ground Eq. (10) reduces to equation (11):

$$k_{obs}^{s} = \frac{k_0 Q_1 f_1 [OX]_T + k_1 Q_1 (f_1 [OX]_T)^2}{1 + Q_1 f_1 [OX]_T (1 + K_2^{/}/[H^+])} \qquad (11)$$

The temperature independent value of Q_1 (= 42.0 dm^3 mol^{-1}) was used, the fraction f_1 was calculated as mentioned above and the k_{obs}^{s} data in Tables S3 and S4 were analyzed by equation (11) using a nonlinear least squares computer program assigning unit weight to each data point. The calculated values of k_0, k_1 and $K_2^{/}$ are collected in Table 2. The k_0 values turned out statistically insignificant. The inclusion of the k_2 term in the calculation did not improve the data fitting. A representative plot at 35°C using a linearized form of Eq. 11 (see Figure 3) clarifies that contributions from k_0, k_2, and k_3 are statistically insignificant.

The k_{obs}^{s} data in Table S2 were then analyzed by Eq. (10) using the values of k_1, $K_2^{/}$ (see Table 2) and Q_1. The calculated values of k_0, k_2 and k_3 are also collected in Table 2. Here again, the k_0 and k_3 values turned out statistically insignificant.

At $5.04 \leq pH \leq 6.72$, and $0.0025 \leq [OX]_T/mol\ dm^{-3} \leq 0.1$, OX^{2-} and HOX^{-} were considered to be the reducing species. The first step acid dissociation equilibrium of *trans*-$Mn^{III}(salen)(OH_2)_2^{+}$ ($pK_M \geq 7.3$[16, 22] was also taken in to account. Eq. (9) was recast as Eq. (12),

$$k_{obs}^{s} = \frac{k_1 Q_1 (f_1 [OX]_T)^2 + k_4 Q_2 f_3 [OX]_T + k^{/} f_1 f_3 [OX]_T^2 + k_6 Q_2 (f_3 [OX]_T)^2}{1 + K_M/[H^+] + Q_1 f_1 [OX]_T + Q_2 f_3 [OX]_T} \qquad (12)$$

285 Table 2. Summary of the calculated values of the rate and equilibrium constants and
286 activation parameters for the redox reaction.

Rate constant [a]	Temp./°C			
	25.0 ± 0.1	30.0 ± 0.1	35.0 ± 0.1	40.0 ± 0.1
k_0 /s^{-1}	0.05 ± 0.0015[b]	0.0045 ± 0.0018[b]	0.00002 ± 0.002[b]	0.00049 ± 0.0029[b]
	0.0000 ± 0.0005[c]	0.000 ± 0.00027[c]	0.000042 ± 0.00025[c]	0.00019 ± 0.00092[c]
k_1 /dm^3 mol^{-1} s^{-1}	0.73 ± 0.12	0.87 ± 0.07	1.16 ± 0.07	1.73 ± 0.24
k_2 /dm^3 mol^{-1} s^{-1}	7.39 ± 1.03	10.4 ± 1.2	19.6 ± 1.4	26.7 ± 4.6
k_3/ dm^3 mol^{-1} s^{-1}	0.00017 ± 0.27	0.00093 ± 0.31	0.13 ± 0.47	0.00013 ± 0.47
$10^6 k_4$ / s^{-1}			0.03 ± 14.0	
k_5 / dm^3 mol^{-1} s^{-1}			0.077 ± 0.047	
10^4 k_6 / dm^3 mol^{-1} s^{-1}			2.94 ± 2.57	
k_7 / dm^3 mol^{-1} s^{-1}			0.077 ± 0.047	
k_8 / dm^3 mol^{-1} s^{-1}				1.08 ± 0.09
$10^4 K_2^{/}$ /mol dm^{-3}	7.14 ± 2.21	4.62 ± 0.54	2.56 ± 0.31	3.52 ± 0.78
Q_1 /dm^3 mol^{-1}	42.0	42.0	42.0	42.0
$\Delta S^{\neq}$ /J K^{-1} mol^{-1}[d]	**k_1 path**	**k_2 path**		
	42.5 ± 6.2	71.7 ± 7.7		
$\Delta S^{\neq}$ /J K^{-1} mol^{-1}[d]	–106 ± 20	+11.7 ± 25.4		

287 [a] rate constants (k_is) are not corrected for the stoichiometry factor (i. e. $k_i$corr = k_i/2).

288 [b] *Calcd.* from the rate data in Table 2. [c] *Calcd.* from the rate data in Tables 3 and 4.

289 [d] Calcd. from the temperature dependence of k_1 and k_2: $k = (k_B T/h)\exp(-\Delta H^{\neq}/RT + \Delta S^{\neq}/R)$.

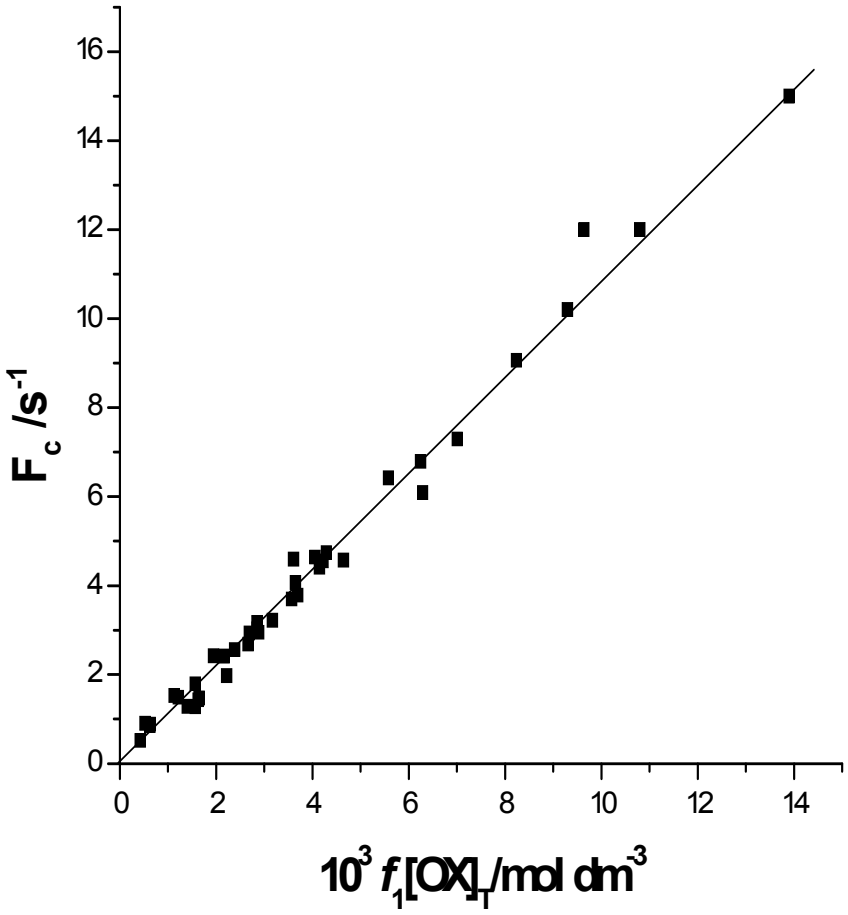

290

291 Figure 3- $10^3\ k_{obs}{}^s(1 + Q_1f_1[OX]_T(1+K_2^{/}/[H^+])/(Q_1f_1[OX]_T)$ (= $\mathbf{F}_c/s^{-1}$) *vs* $10^3f_1[OX]_T$ /mol dm^{-3}
292 plot at 35°C.

293

294 and $k_{obs}{}^s$ values in Table S5 were analyzed by equation (12) with the known values of Q_1, k_1
295 and the calculated value of Q_2 (= $Q_1K_2^{/}/K_2$); pK_M was varied between 6.8 - 7.3. The
296 calculated values of k_4, $k^{/}$ (= $k_5Q_2 + k_7Q_1$) and k_6 turned to be little sensitive to pK_M.

297 2.5.3 *Effect of Ionic strength*

298 The ionic strength was varied as $0.01 \leq \boldsymbol{I}$/ mol $dm^{-3} \leq 0.3$ at 30°C keeping pH = 3.73 ±
299 0.06 and $[OX]_T$ = 0.006 mol dm^{-3}. The values of $k_{obs}{}^s$ did not change significantly with the

variation of ionic strength and averaged to (3.52 ± 0.09) x 10^{-4} s^{-1}. This is as expected from the consideration that under this condition, the redox process is essentially driven by the reaction between the uncharged Mn^{III} complex and the anion, HOX^{-} (i.e. $Mn^{III}(Salen)(OH_2)(HOX)^0 + HOX^{-}$, see Scheme 2). No detailed analysis of the ionic strength effect was further attempted considering the complexity of the reaction.

2.5.4 *Effect of acrylamide*

The oxidation of oxalate by Mn^{III} and its complexes including $Mn^{III}OX^{+}$ is known to generate the oxalate radical, $C_2O_4^{-\cdot}$ which decomposes in a fast step to yield the radical $CO_2^{-\cdot}$ and CO_2.[18, 23] Recently the computer simulation of the complex oxalic acid permanganate reaction which involve the oxalate complexes of Mn^{III} unearthed the less known crucial role of the radical $CO_2^{-\cdot}$. [24] The dimerisation of $CO_2^{-\cdot}$ is also fast and regenerates oxalate. If this is a major step of the loss of $C_2O_4^{-\cdot}$ then the overall stoichiometry of the reaction of Mn^{III} complex with $OX^{2-}/HOX^{-}/H_2OX$ will be 1:1. On the other hand, the overall stoichiometry 2:1 for Mn^{III}/OX_T reaction should result if Mn^{III} complex scavenges the radical ($C_2O_4^{-\cdot}$ / $CO_2^{-\cdot}$) at a rate much faster than the rate of its dimerisation. Keeping that in mind we investigated the effect of acrylamide monomer, a good scavenger of the radical, on the kinetics of the reaction under study at 30°C with $[Mn^{III}(salen)(OH_2)_2^{+}]_T$ = 1.21 x 10^{-4}, $[OX]_T$ = 2.5 x 10^{-3}, $\boldsymbol{I}$ = 0.3 mol dm^{-3} and pH = 3.22. The anticipated polymer formation (through visual inspection) could not be observed. Interestingly the values of k_{obs}^{s} showed a decreasing trend with the increase of $[acrylamide]_T$ ($10^4 k_{obs}^{s}/s^{-1}$ = 1.67 ± 0.02, 1.63 ± 0.02, 1.61 ± 0.02 and 1.57 ± 0.02 at $[acrylamide]_T$(monomer) = 0, 0.01, 0.02, 0.03 mol dm^{-3} respectively). This indirectly led us to believe that the Mn^{III} complexes compete very successfully and efficiently in scavenging the $C_2O_4^{-\cdot}$ or $CO_2^{-\cdot}$ generated in the redox process maintaining the stoichiometry (=$|\Delta[Mn^{III}]|/|\Delta[OX]|$): 2 :1, and dimerisation of $CO_2^{-\cdot}$ at high dilution is of little significance; the possible reason may be the role played by the coulombic repulsion between the anionic

radicals in relation to the favorable electrostatic and non covalent interactions (*H*-bonding) between the radical anion and $Mn^{III}(salen)(OH_2)_2^+$ and $Mn^{III}(salen)(OH_2)(OXH)$.

2.5.5 *Effect of Surfactant, Sodium dodecyl sulphate(SDS)*

The UV-Vis absorption spectra of *trans*-$Mn^{III}(salen)(OH_2)_2^+$ in the presence of varying [SDS] ($[complex]_T$ = 5.70 x 10^{-5}, $[HClO_4]$ =1.0 x 10^{-4} $[SDS]_T$ = 0, 0.01, 0.02, 0.05,0.10 mol dm^{-3}, $260 \leq \lambda$, nm ≤ 500, see Figure S4a) exhibits a small red shift (~ 2nm) and are virtually super imposable except for [SDS] = 0 (the spectral measurements at $[SDS]_T$ = 0.002 – 0.006 could not be made due to appearance of a silky white precipitate). Only a small reduction in intensity (≤ 4% decrease of absorbance at 280 nm) is observed due to the presence of the surfactant. The fluorescence spectra of $Mn^{III}(salen)(OH_2)_2^+$ in aqueous SDS media ($[SDS]_T$/mol dm^{-3} = 0, 0.02, 0.03, 0.05) is presented in Figure S4(b). The emission peak is observed at 415 nm in absence of SDS; it is enhanced with the increase of [SDS] indicating micellar binding of $Mn^{III}(salen)(OH_2)_2^+$. The observed trends in emission and absorption behavior of $Mn^{III}(salen)(OH_2)_2^+$ are reconciled with the partitioning of this cationic complex from the bulk aqueous phase to the dominantly water rich region of the micellar surface.

The rate data (k_{obs}^s, 30°C) at constant $[OX]_T$ = 0.006 mol dm^{-3}, pH = 3.97 ± 0.03 and 0.00 ≤ $[SDS]_T$/mol dm^{-3} ≤ 0.10 are collected in Table S6. There is no significant effect of [SDS] on the rate constant at $[SDS]_T \leq 0.0075$ mol dm^{-3}; marked retardation is observed beyond $[SDS]_T$ = 0.0075 mol dm^{-3} and k_{obs}^s tends to attain a low limiting value at high [SDS]. This is reconciled with the fact that the diaqua complex and presumably the neutral complex, *trans*- $Mn^{III}(salen)(OH)_2(OXH)$, are partitioned into the micellar pseudo phase of SDS and this protects the Mn^{III} species from electron transfer involving HOX^- which on electrostatic ground exists exclusively in the aqueous pseudo phase. The pH condition is such

that $[OX]_T$ exists in equilibrium in the bulk aqueous phase as HOX^- and OX^{2-}. Interestingly there is substantial rate enhancement on increasing $[Na^+]_T$ by addition of $NaClO_4$ (= 0.01 – 0.3, see Table S6) at a fixed $[SDS]_T$= 0.02 which also leads to the decrease of pH. The observed pH perturbation is a clear indication of the prevalence of ion exchange equilibrium involving H^+/Na^+ between the anionic micellar pseudo phase and the bulk aqueous phase. We consider the participation of the mono cationic Mn^{III} complex in this ion exchange equilibrium along with the equilibrium partitioning of the corresponding neutral HOX complex between the bulk aqueous phase and micellar pseudo phase. Scheme 3 is presented to interpret the rate data. Accordingly,

$$k_{obs}^{s} = \frac{k_{1W} Q_1^0 y_+^2 [HOX^-_W]^2}{1 + Q_1^0 (y_+^2 + K_2^{0/}/[H^+_W])[HOX^-_W] + K_{ex}([Na^+]_M/[Na^+]_W) + Q_m Q_1^0 y_+^2 [HOX^-]_W [Dn]} \quad (13)$$

where Q_1^0, $K_2^{0/}$ are the corresponding terms at zero ionic strength, y_+ is the activity coefficient of a mono valent cation, $[Na^+_M] = \beta\,[Dn] - [H^+_M]$, $[H^+_M] = [H^+]_T - [H^+_W] - [OX]_T[H^+_W]/([H^+_W]+K_2^0/y_+^2)$, $[Dn] = [SDS]_T$ – cmc, cmc denotes critical micelle concentration, the subscripts M and W stand for the micellar pseudo-phase and bulk aqueous phase respectively (the micellar binding parameter β is approximated to : $\beta = ([Na^+_M] + [H^+_M])/[Dn]$ as $[Na^+_M] + [H^+_M] \geq [R^+]_M + ROXH_M$), $R^+ = Mn^{III}(salen)(OH_2)_2^+$. The ionic strength ($\boldsymbol{I}$) of the aqueous pseudo phase,

$$\boldsymbol{I} = 3[Na_2OX]_T + [NaHOX]_T + [NaClO_4] + cmc + 0.5(1-\beta)[[SDS]_T - cmc)$$

was calculated neglecting the contribution from $[Mn^{III}(salen)(OH_2)_2]^+_W$ ($[complex]_T$ = 1.0-1.2 x 10^{-4} mol dm^{-3}). The activity coefficient at a given ionic strength was calculated using the relationship,

$$\log y_{z+} = -0.5\, Z^2\, (\boldsymbol{I}^{1/2}/(1+\boldsymbol{I}^{1/2})) + 0.2\,\boldsymbol{I} \quad (14)$$

where Z denotes the charge of the ionic species. Since the solution compositions had variable ionic strength, the values of the equilibrium parameters (Q_1, K_2, $K_2^{/}$) used in the data fitting were corrected to zero ionic strength. The rate data (k_{obs}^{s}) at $0.01 \leq [SDS]_T/mol\ dm^{-3} \leq 0.1$ were analyzed by Eq. (13) with $k_{1w} = k_1$, $pK_2^0 = 4.27$ [21], $Q_1^0 = 72.7$ ($= Q_1(\boldsymbol{I} = 0.3)/ y_+^2$ for $y_+ = y_-$) by varying cmc and β.

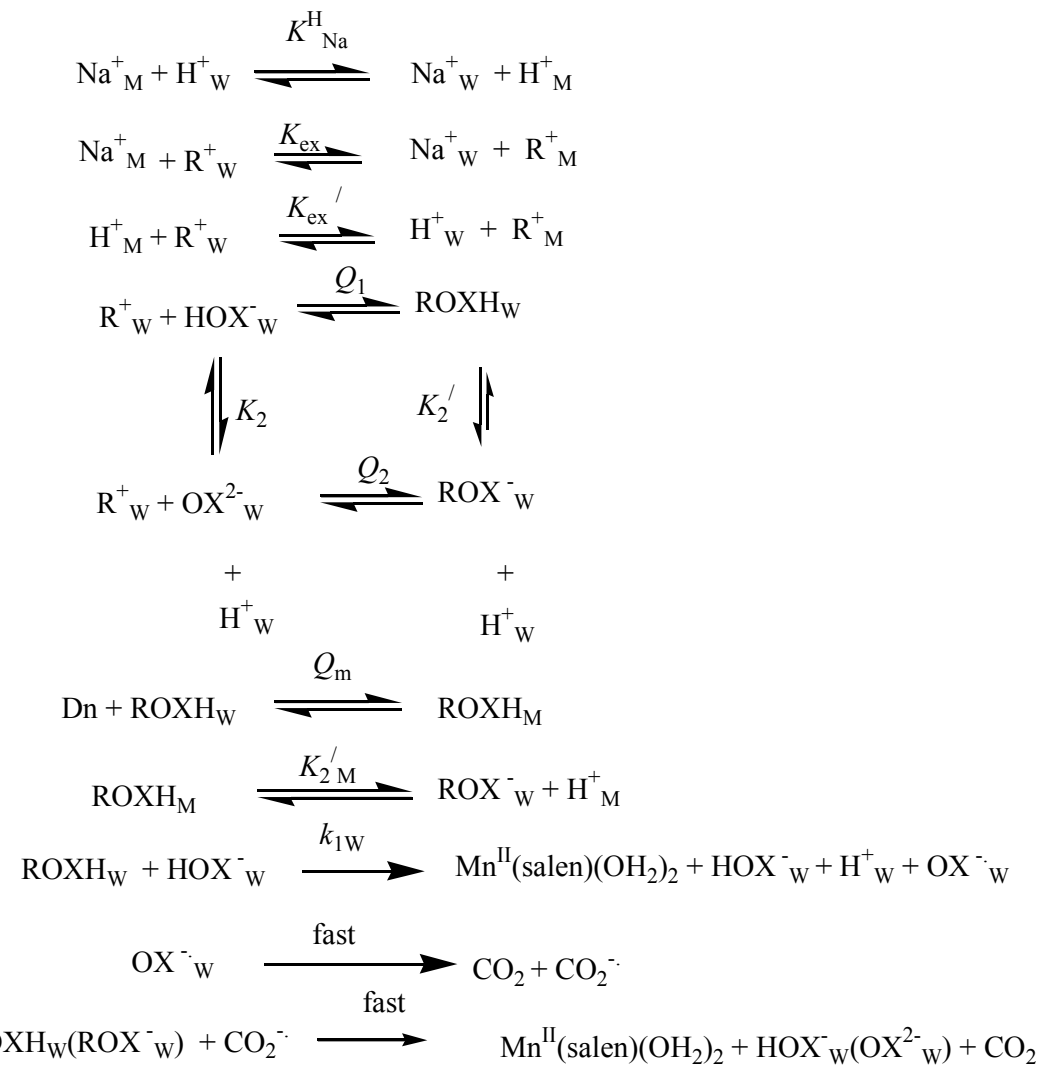

Scheme 3 - $Mn^{III}(salen)(OH_2)_2^+$ reduction by HOX^- in the presence of SDS micelles, $R^+ = Mn^{III}(salen)(OH_2)_2^+$, $Dn = [SDS]_T$ - cmc

The best fit values of K_{ex}, β and cmc turned out as 10.4 ± 0.8, 0.6 and 0.009 (cmc = 0.008 mol dm^{-3} at 25°C, in absence of additives)[25] respectively while the micellar binding constant Q_m for the partitioning of the neutral species, $Mn^{III}(salen)(OH_2)(HOX)$, is statistically insignificant (see Table S6, and Table S7).

2.5.6 *Effect of azide (N_3^-)*

The effect of azide ion on the redox reaction was studied at 40°C with $0.01 \leq [NaN_3]_T/mol\ dm^{-3} \leq 0.2$ at fixed $[OX]_T = 0.022$, $\boldsymbol{I}$ = 0.3 mol dm^{-3} and constant pH = 4.53 ± 0.03. k_{obs}^s increases with $[N_3^-]_T$ tending to attain a limiting value (see Table S8).

This trend is explicable in terms of the equilibrium formation of *trans*-$Mn^{III}(salen)(OH_2)(N_3)$ competitive with the corresponding HOX^- complex followed by the reduction of the azido complex by oxalate species as given below. Accordingly k_{obs}^s is given by Eq. (15)

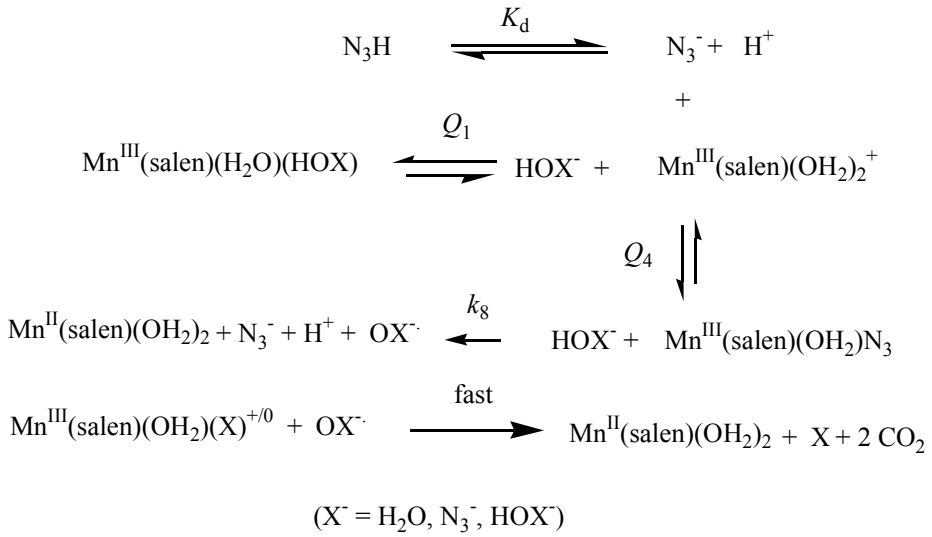

$$k_{obs}^{s} = \frac{k_{obs}^{/} + k_8 Q_4 f_1 [OX]_T([N_3^-]/G)}{1 + Q_4([N_3^-]/G)} \qquad (15)$$

where $G = 1.0 + Q_1[HOX^-](1+K_2^{/}/[H^+])$, $[N_3^-] = K_d[N_3^-]_T/([H^+] + K_d)$ (pK_d = 4.35 at 25°C, $\boldsymbol{I}$ = 0.3 mol dm^{-3} for N_3H)[26] and $k_{obs}^{/} = k_{obs}^{s}$ in absence of azide. The k_{obs}^s data fitted Eq. (15)

well and the values of k_8 and Q_4 are collected in Table S8. As a check a preliminary rate measurement for the reduction of $Mn^{III}(salen)(OH_2)_2^+$ by N_3^- ($[N_3^-]_T$/mol dm^{-3} = 0.01, 0.10 and 0.2) indicated that such reaction at 40^{o}C, pH = 4.46 ± 0.06 (I = 0.3 mol dm^{-3}) was extremely slow (see absorbance versus time plots in Figure S_5) yielding k_{obs}^s = (7.7 ± 0.3) x 10^{-6} s^{-1} for $[N_3^-]_T$ = 0.2 mol dm^{-3}.

2.5.7 *Molecular Modelling and Structure Optimization*

All calculations were performed with the program package TURBOMOLE 6.4 using density functional theory (DFT).[27,28] The BP86 functional and def2-TZVPP basis set together with the resolution-of-the-identity (RI) approximation[29-31] (RI-BP86/def2-TZVPP in short) was employed for the structure optimization procedure. Numerical frequency calculations of the optimized structures were done to ensure that the optimized structures were true minima not the transition states. The "freeh" script of turbomole was used to calculate the free energies of the complexes at 25^{o}C (298 K) and 1 atmospheric pressure. For the graphical presentation and the bond distance and angle measurements Mercury 3.0 was used.[32]

3.1 *Results and Discussion*

3.1.1 *Formation/dissociation of trans-Mn^{III}(salen)(OH_2)(HOX)*

The kinetic data could not detect outer sphere association of the diaqua Mn^{III} complex with HOX^- or H_2OX. Also H_2OX is not an effective reactant for the aqua ligand substitution (k_2^f ~ 0, see Table S1c) at the Mn^{III} centre. Similar observation has been reported for hydroquinone/catechol (H_2Q/H_2Cat).[22] However, such a path has been detected for ascorbic. The comparison made in Table 1 reflects the dependence of the rate constants on the nature of the incoming ligand and the electrostatic interaction between the reacting partners. The rate constants may be contrasted with the water exchange rate constant of $[Mn^{III}(OH_2)_6]^{3+}$, $k_{ex} \sim 10^5$ s^{-1}. [34] The labilizing effect of the coordinated hydroxide (see Table 1) is not large.

Similar behaviour has been recently reported for the water exchange reactions of *trans*-(diaqua)/(aqua/hydroxo) Mn^{III}(porphyrins) (at 25°C values of k_{ex} /s^{-1}, $\Delta H^{\neq}$/kJ mol^{-1}, $\Delta S^{\neq}$/J K^{-1} mol^{-1} for *trans*- $[Mn^{III}(TPPS)(OH_2)_2]^{3-}$ and its (aqua)(hydroxo) isomer are: (1.4 ± 0.1) x 10^7, 32.7 ± 1.1, 1.65 ± 3.0 and (2.5 ± 0.7) x 10^7, 24.1 ± 2.0, –22.9 ± 9.9 respectively). [35] The $\Delta H^{\neq}$ values for the formation and dissociation of HOX complex are similar in magnitude ($\Delta\Delta H^{\neq}(k_1^f - k_{-1}^f)$ = -9.6 ± 6.7 kJ mol^{-1}). This is expected as the bond that is broken and reformed in the process are alike (i.e. Mn^{III}-O). However, a higher value of $\Delta H^{\neq}$ for the reverse reaction (k_{-1}^f) may be reconciled with the relatively stronger columbic interaction of the outgoing HOX^- with the Mn^{III} centre. Such a trend is not seen in the activation enthalpy data for the reversible formation of the anionic azido complex, $Mn^{III}(EDTA)(N_3)^{2-}$ (see Table 1) reported by Suwyn and Hamm.[36] Strikingly the activation entropies for the formation and dissociation of *trans*-$[(OH_2)Mn^{III}(salen)(HOX)]$ (see Table 1) are virtually the same and moderately negative ; similar trend is also observed for $Mn^{III}(EDTA)N_3^{2-}$. This leads us to suggest an associative transition state (***t. s.***, I_a mechanism) involved in the aqua ligand substitution at the Mn^{III} centre.

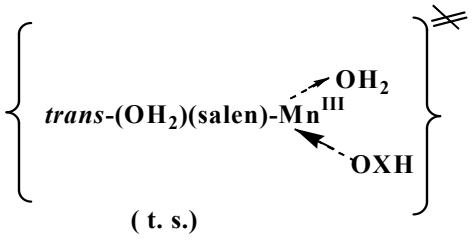

The seven coordinate Mn^{III} centre in the transition state does not seem to be unusual considering the seven coordinate complexes, $Mn^{III}(EDTA)(OH_2)^-$ and $Mn^{III}(EDTA)(N_3)^{2-}$ reported by Suwyn and Hamm.[36]

3.2.2 *Redox Reaction*

In the context of the redox reaction it is pertinent to discuss the DFT optimized structures of different oxalato complexes and their structural parameters. Figure 4 depicts the structures of *trans*-Mn^{III}(salen)(OH_2)(HOX)(**A**), Mn^{III}(salen)$(HOX)_2^-$(**B**) and Mn^{III}(Salen)(OH_2)$(OX)^-$ (**C_1** and **C_2** , the two isomeric forms with respect to the disposition of H_2O).

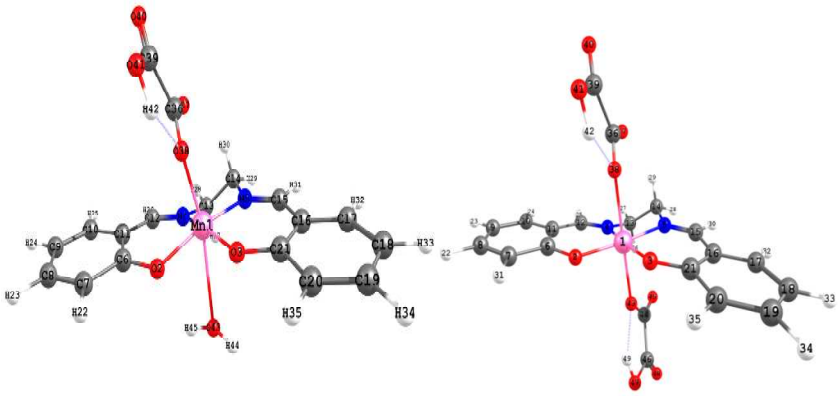

A **B**

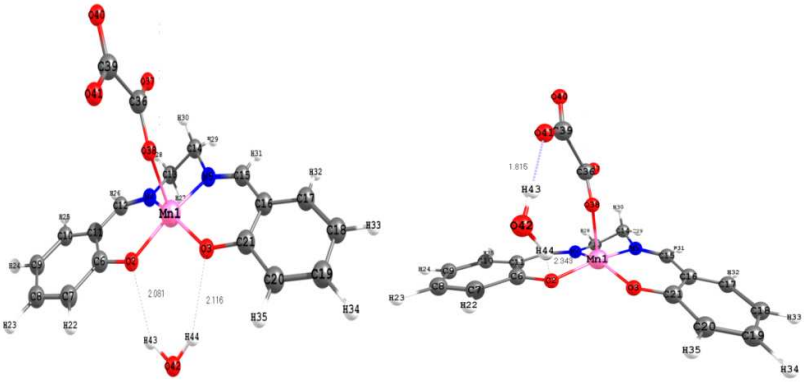

C_1 **C_2**

Figure 4. RI-BP86/def2-TZVPP optimized structures of *trans*- Mn^{III}(salen)(OH_2)(HOX) (**A**), Mn^{III}(salen)$(HOX)_2^-$(**B**), and Mn^{III}(salen)(OH_2)$(OX)^-$ (**C_1**,**C_2**), HOX^-(OX^{2-}) denotes $^-$O-C(=O)CO_2H/$^-$O-C(=O)CO_2^-.

457 Table 3. Selected bond distances (Å) and bond angles (deg) for **RI-BP86/def2-TVZPP**

458 optimized structures of *trans*- Mn^{III}(salen)(OH_2)(HOX) (**A**), Mn^{III}(salen)$(HOX)_2^-$ (**B**) and

459 Mn^{III}(salen)(OH_2)$(OX)^-$ (**C_1, C_2**).

A	**B**	**C_1**	**C_2**
Bond distances (Å)			
Mn-O(2 phenoxide) 1.909	Mn-O(2 phenoxide) 1.908	Mn-O(2 phenoxide) 1.913	Mn-O(2 phenoxide) 1.900
Mn-O(3 phenoxide) 1.895	Mn-O(3 phenoxide) 1.908	Mn-O(3 phenoxide) 1.921	Mn-O(3 phenoxide) 1.909
Mn-O(43 W) 2.895	Mn-O(43 O-$COCO_2H$)2.257	Mn-O(42 W) too long	Mn-O(42 W) too long
Mn-O(38 O-$COCO_2H$) 2.080	Mn-O(38 O-$COCO_2H$) 2.257	Mn-O(38 O-$COCO_2^-$) 2.020	Mn-O(38 O-$COCO_2^-$) 2.003
Mn-N(4 imine) 1.992	Mn-N(4 imine) 2.00	Mn-N(4 imine) 1.984	Mn-N(4 imine) 1.993
Mn-N(5 imine) 1.990	Mn-N(5 imine) 2.00	Mn-N(5 imine) 1.963	Mn-N(5 imine) 1.967
O(38)….H(42) 1.867	O(38)….H(42) 1.784	O(2 phenoxide)….H(43 W) 2.081	O(3 phenoxide)….H(44 W) too long
	O(43)….H(49) 1.784	O(3 phenoxide)….H(44 W) 2.116	O(2 phenoxide)….H(44 W) 2.343
			O(41 O-COCO2)…H(43 W) 1.815
Bond Angles (deg)			
O(2)-Mn-O(38) 95.1	O(2)-Mn-O(38) 89.2	O(2)-Mn-O(38) 96.7	O(2)-Mn-O(38) 95.9
O(2)-Mn-O(3) 93.7	O(2)-Mn-O(3) 95.3	O(2)-Mn-O(3) 93.1	O(2)-Mn-O(3) 92.5
O(2)-Mn-N(4) 89.6	O(2)-Mn-N(4) 91.1	O(2)-Mn-N(4) 89.9	O(2)-Mn-N(4) 90.5
O(3)-Mn-N(5) 90.8	O(3)-Mn-N(5) 91.1	O(3)-Mn-N(5) 90.3	O(3)-Mn-N(5) 90.3
O(2)-Mn-N(5) 164.8	O(2-Mn-N(5) 173.5	O(2-Mn-N(5) 166.7	O(2-Mn-N(5) 167.5
O(3)-Mn-N(4) 163.9	O(3)-Mn-N(4) 173.5	O(3)-Mn-N(4) 159.9	O(3)-Mn-N(4) 157.3
O(3)-Mn-O(43) 81.6	O(3)-Mn-O(43) 89.2		
O(2)-Mn-O(43) 71.0	O(2)-Mn-O(43) 91.7		
N(4)-Mn-N(5) 82.3	N(4)-Mn-N(5) 82.5	N(4)-Mn-N(5) 82.6	
N(4)-Mn-O(38) 97.1	N(4)-Mn-O(38) 89.5	N(4)-Mn-O(38) 96.5	N(4)-Mn-O(38) 97.6
N(4)-Mn-O(43) 84.6	N(4)-Mn-O(43) 89.4		

N(5)-Mn-O(38) 98.7	N(5)-Mn-O(38) 89.4	N(5)-Mn-O(38) 95.0	N(5)-Mn-O(38) 95.2
N(5)-Mn-O(43) 95.3	N(5)-Mn-O(43) 89.5		
Mn-O(2)-C(6) 126.1	Mn-O(2)-C(6) 129.3	Mn-O(2)-C(6) 129.3	Mn-O(2)-C(6) 129.8
Mn-O(3)-C(21) 131.2	Mn-O(3)-C(21) 129.3	Mn-O(3)-C(21) 130.9	Mn-O(3)-C(21) 131.2
Mn-N(4)-C(12) 124.7	Mn-N(4)-C(12) 125.7	Mn-N(4)-C(12) 126.2	Mn-N(4)-C(12) 126.1
Mn-N(5)-C(15) 126.6	Mn-N(5)-C(15) 125.7	Mn-N(5)-C(15) 127.8	Mn-N(5)-C(15) 127.8

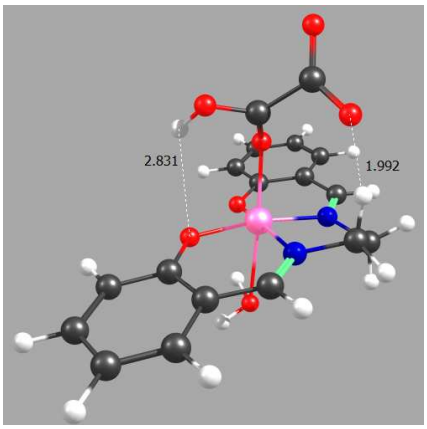

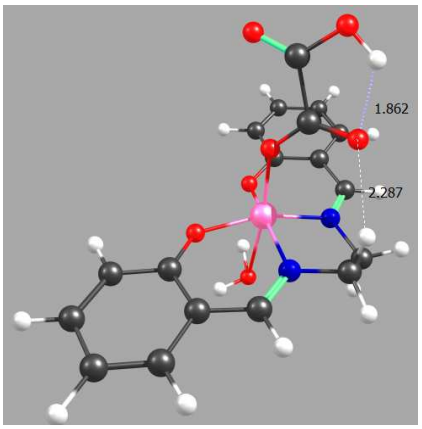

EH = -2484.197488812 (78.7 kJ/mol) EH = -2484.227449387 (0 kJ/mol)

D_1 **D_2**

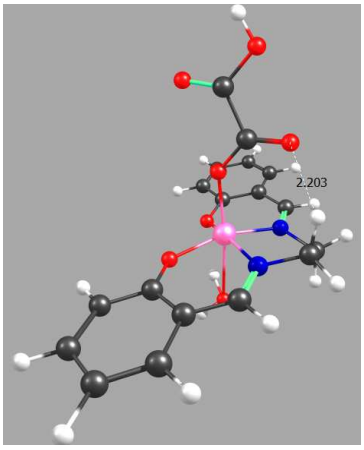

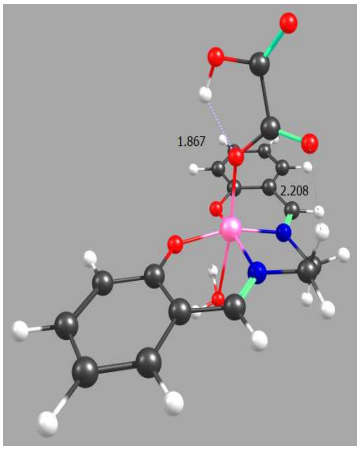

EH = -2484.219320944 (21.3 kJ/mol) EH = -2484.226175044 (3.3 kJ/mol)

D_3 **D_4**

Figure 5 - RI-BP86/def2-TZVPP optimized structures of *trans*-Mn^{III}(salen)(OH_2)(HOX), D_1- D_4 denote the hydrogen bonded conformational isomers.

Relevant bond distances and bond angles are collected in Table 3. In all these structures, the (N_2, O_2) square plane around Mn^{III} suffers little distortion while the axial Y-Mn^{III}-X bonds are strongly distorted and also differently for **A**, **B**, and $\mathbf{C_1}$, $\mathbf{C_2}$. For example the Mn-O (38 O-$COCO_2H$) bond in **A** is 0.177 Å shorter than the same in **B**. Also the Mn-O (43W) bond for the *trans* H_2O in **A** is substantially elongated (2.895 Å). The free carboxyl group(s) in both **A** and **B** are bridged to the boned carboxylate group(s) through hydrogen bonds with a relatively shorter *H*- bond length ($\delta_{(H\text{-bond})B\text{-}A}$ = 0.083 Å) for **A**. This might be traced to the relatively stronger binding of HOX^- to Mn^{III} in **A** in tune with comparatively shorter Mn-O bond length (38 O-$COCO_2H$) in this case. In all such structures Mn^{III} is situated above the partially distorted (N_2, O_2) square frame of the salen motif. The computed structures of *trans*-Mn^{III}(salen)(OH_2)(HOX) with possible *H*-bonding of the O-H function of the unbound carboxyl group are depicted in $\mathbf{D_1}$- $\mathbf{D_4}$ (Figure 5). It turns out that $\mathbf{D_1}$ with a long hydrogen bond (O---H bond 2.831Å) between the phenoxide oxygen and the free carboxyl group is energetically unfavourable; $\mathbf{D_2}$ (same as A in Figure 4) is the most acceptable one.

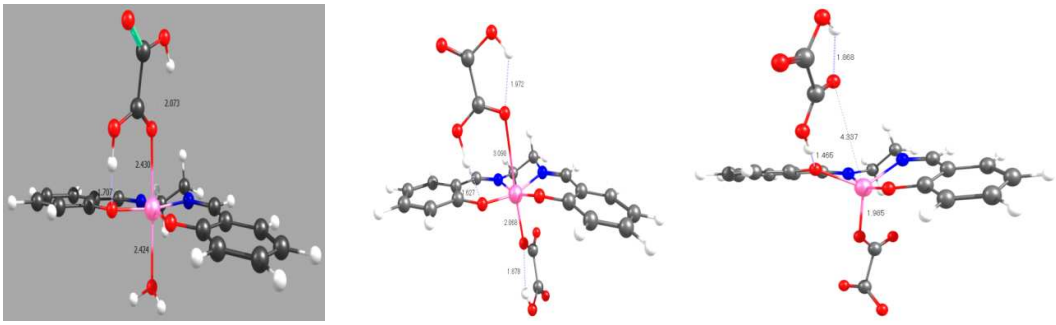

$\mathbf{E_1}$ $\mathbf{E_2}$ $\mathbf{E_3}$

Figure 6**.** RI-BP86/def2-TZVPP optimized structures of *trans*- Mn^{III}(salen)(OH_2)$(H_2OX)^+$ ($\mathbf{E_1}$), Mn^{III}(salen)(HOX)(H_2OX) ($\mathbf{E_2}$), and Mn^{III}(salen)(OX)(H_2OX) ($\mathbf{E_3}$); H_2OX is oxalic acid molecule, and HOX^-, OX^{2-} denote its mono- and di- anions respectively .

Notable is the fact that OX^{2-} coordination to Mn^{III} leads to very strong axial distortion resulting in expulsion of the bound H_2O from the Mn^{III} centre (**C_1, C_2**). Essentially Mn^{III} in *trans*-$Mn^{III}(salen)(OH_2)(OX)^-$ assumes five coordination. Figure 6 depicts the computed structures of *trans*-$Mn^{III}(salen)(OH_2)(H_2OX)^+$(**$E_1$**), $Mn^{III}(salen)(HOX)(H_2OX)$ (**E_2**), and $Mn^{III}(salen)(OX)(H_2OX)^-$(**$E_3$**). In **$E_1$** oxalic acid ($H_2OX$) molecule is bound to Mn^{III} centre by C=O function with long Mn-O bond (2.430Å); one *H*-bond between the phenoxide group and the carboxyl proton (H---O bond 1.707 Å) of the bound carboxyl group completes a six membered ring structure imparting stability. It may be noted that both the M-O bond lengths *trans* to each other do not differ significantly although they are assembled differently (H_2O-Mn-O=C-). In **E_2** the hydrogen bond length between the phenoxide oxygen and the carboxylic proton decreases to 1.627Å with elongation of the Mn^{III}-O bond of Mn^{III}-O=C- to 3.090 and concurrent compression of the *trans*-Mn^{III}-O (Mn^{III}-OXH) to 2.068 Å. Interestingly H_2OX in **E_3** is *H*-bonded to the phenoxide group (O---H = 1.465Å) with a long Mn^{III}-O distance (4.337 Å) of Mn^{III}-O=C (no bonding situation) with simultaneous shortening of the *trans*-Mn-O (1.986 Å) reflecting the strong *trans* effect of the coordinated OX^{2-}. Although these computationally accessible species, $Mn^{III}(salen)(X)(H_2OX)^+$ (X = H_2O, HOX^- and OX^{2-}) are not experimentally identified in aqueous medium, they provide sufficient insight to understand the reaction mechanism. Thus the computational study shows that there is a possibility of inner sphere reduction of Mn^{III} by HOX^- and H_2OX in the reactions of $Mn^{III}(salen)(OH_2)(HOX)$ with HOX^- and H_2OX (k_1 and k_2 paths). The corresponding reactions between *trans*-$Mn^{III}(salen)(OH_2)(OX)^-$ and HOX^- (k_5 path), *trans*-$Mn^{III}(salen)(OH_2)(OX)$ and OX^{2-} (k_6 path), and *trans*-$Mn^{III}(salen)(OH_2)(HOX)$ + OX^{2-} (k_7 path) in all probability be considered as outer sphere type as coordination of OX^{2-} to Mn^{III} will lead to the displacement of the *trans*- ligand (**C_1** and **C_2**) due to the predominant structural *trans* effect (**STE**) of OX^{2-}.

We observe that the intramolecular electron transfer reactions from the bound oxalate to Mn^{III} centre in *trans*- $Mn^{III}(salen)(OH_2)(HOX)$ (k_0) and $Mn^{III}(salen)(OH_2)(OX)^-$ (k_4) are too slow, if at all occur, under the experimental conditions. This is what we observed in an earlier study of the reduction of Mn^{III} by the bound glyoxylate (gem diol form) in *trans*-$Mn^{III}(salen)(OH_2)(O_2CH(OH_2)_2$ ($10^5 k_0$/ s^{-1} = 0.05 ± 0.53 at 45°C). [17] For such complexes the values of their formation equilibrium constant {Q_1/mol dm^{-3} = 33.2-25.0, 42.0, 49.5 (25-40°C, ***I*** / mol dm^{-3}= 0.3) for $CH(OH)_2CO_2^-$, HOX^- and OX^{2-}respectively} and the p$K^{/}$ data (–log $K^{/}$= 3.38 ± 0.20 see Table 2) of $Mn^{III}(salen)(OH_2)(HOX)$ suggests that the carboxylate ligand binds the Mn^{III} centre in a monodentate fashion; this is further supported on a comparative basis by a value of pK = 2.0 (28°C, ***I*** = 0.3 mol dm^{-3}) for the unbound carboxyl group of bioxalatopentaamminecobalt(III), $(NH_3)_5CoOCOCO_2H^{2+}$.[37] Despite this fact the carboxylate ligand binding results in substantial stabilization of the Mn^{III} state towards intramolecular redox process. The DFT calculations indicate that there is a finite possibility of a 1:1 species, $Mn^{III}(salen)(H_2O)(H_2OX)^+$. We, however, did not observe [H_2OX] dependent rate of complexation of $Mn^{III}(salen)(OH_2)_2^+$. Also the rate constant of reduction of $Mn^{III}(salen)(OH_2)_2^+$ by H_2OX (k_3) turned out statistically insignificant. The possible reason for not being able to detect $Mn^{III}(salen)(H_2O)(H_2OX)^+$ is due to the very low pK_1 of oxalic acid (pK_1 = 1.0 - 1.04 at 20°-40° C). Further lowering of the pK_1 of the coordinated oxalic acid favours complete H^+ dissociation under the experimental conditions and in consequence $Mn^{III}(salen)(OH_2)(H_2OX)^+$, if formed, gets converted to its HOX analogue. Presumably the experimental identification of $Mn^{III}(salen)(OH_2)(H_2OX)^+$ in aqueous medium demands still higher [H^+] and [H_2OX]. However, the acid catalyzed decomposition of $Mn^{III}(salen)(OH_2)_2^+$ at high [H^+] set a limit to our investigation to [H^+] ≤ 0.05 mol dm^{-3}.

The predominant reactions are the reduction of Mn^{III} in $Mn^{III}(salen)(OH_2)(HOX)$ by HOX^- (k_1 path) and H_2OX (k_2 path), H_2OX being a better reducing agent than HOX^- (k_2/k_1 ≥

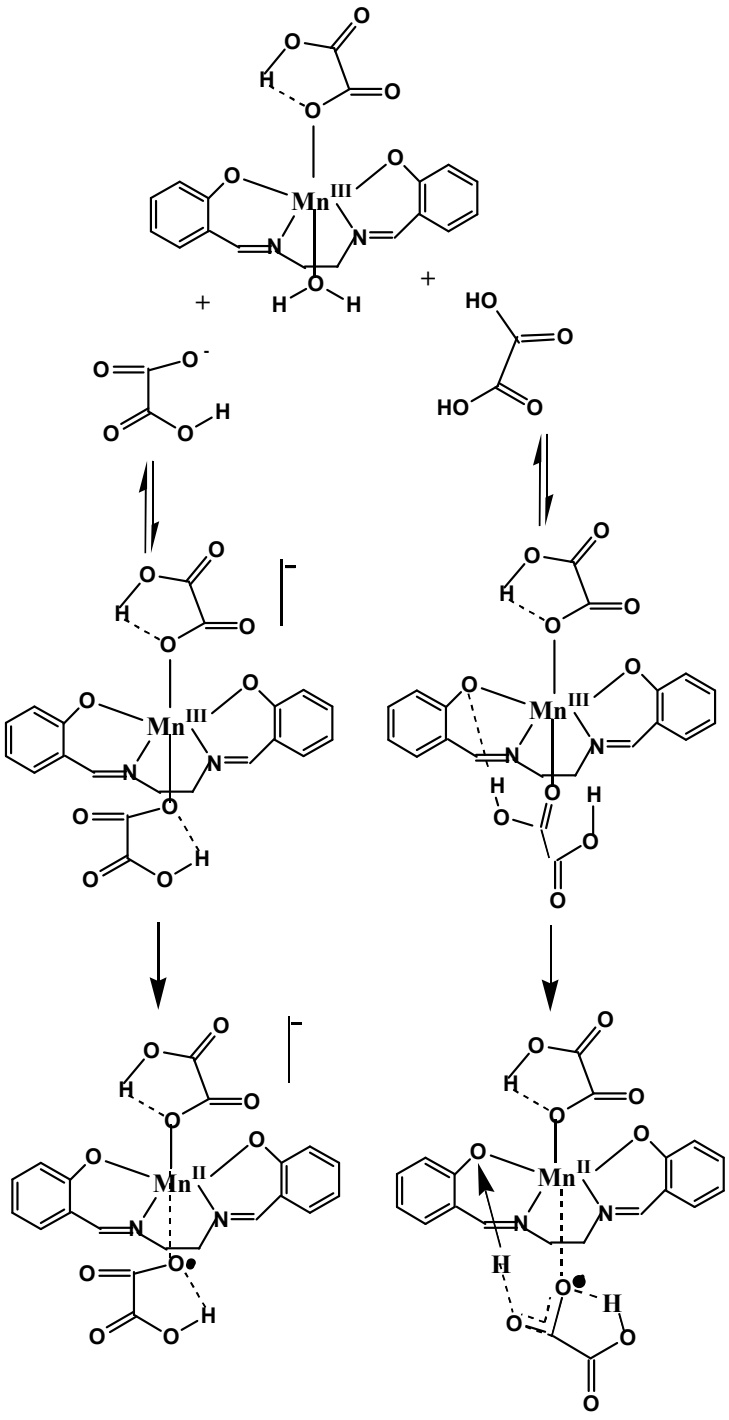

Figure 7 – Probable mechanism of Proton coupled electron transfer (PCET) involved in k_1 and k_2 paths.

10 at 25-40°C). This trend appears surprising as HOX^- is a better electron donor than its conjugated acid, H_2OX. To account for this difference we suggest that the reaction in the k_2 path is preferably an efficient inner-sphere electro-protic reaction involving proton coupled electron transfer, PCET, (Figure 7) or concerted proton electron transfer, CPET, process as observed in the oxidation of aromatic phenols by $Mn^{III}(OH)(dpaq)^+$ (dpaq = 2-[bis(pyridine-2-ylmethyl)]amino-N-quinolin-8-yl-acetamidate) in MeCN.[38]

Substantially large differences in the activation enthalpy ($\Delta\Delta H^{\neq}_{(k2\,-\,k1)}$ = 29.2 ± 9.3 kJ mol^{-1}) and entropy ($\Delta\Delta S^{\neq}_{(k2\,-\,k1)}$ = +117.5 ± 32.4 J K^{-1} mol^{-1}) are observed for the two paths. The observed activation enthalpy arises due to (i) the enthalpy changes associated with the pre-equilibria, and (ii) energy demand for the rearrangement of bonds in the activation process. Out of these two contributing factors the later will predominate as the nature of the bond broken and reformed in the equilibrium pre-association are alike (Mn^{III}-O). However, the $\Delta S^{\neq}$ term depends on solvation of the reacting species in the initial states and the transition states. In the present case the substantially negative value of the activation entropy for k_1 path might indicate the involvement of an ordered transition state. There is likely to be much greater degree of rearrangement of bonds in the k_2 path (see Figure 7) which accounts for the relatively higher values of $\Delta H^{\neq}$ and $\Delta S^{\neq}$ for this path. A simple calculation of the thermodynamic parameters for the k_1 and k_2 paths, $[X(TS_2^{\neq}) - X(TS_1^{\neq})]$, where X = G, H, S and $TS_2^{\neq}$ and $TS_1^{\neq}$ denote the activated states for the electron transfer respectively might clarify this picture. The differential values of the thermodynamic parameters can be expressed as,

$$\boldsymbol{G}(TS_2^{\neq}) - \boldsymbol{G}(TS_1^{\neq}) = -2.303RT[pK_1 + \log k_2/k_1] + \mathbf{G}^0(H^+)$$

$$\boldsymbol{H}(TS_2^{\neq}) - \boldsymbol{H}(TS_1^{\neq}) = \Delta H^{\neq}(k_2) - \Delta H^{\neq}(k_1) - \Delta H^0(K_1) + \boldsymbol{H}^0\,(H^+)$$

$$\boldsymbol{S}(TS_2^{\neq}) - \boldsymbol{S}(TS_1^{\neq}) = \Delta S^{\neq}(k_2) - \Delta S^{\neq}(k_1) - T^{-1}\Delta H^0(K_1) + 2.303R\ pK_1 + \boldsymbol{S}^0\,(H^+)$$

where $\boldsymbol{X}^0(H^+)$ ($\boldsymbol{X}$ = $\boldsymbol{G}$, $\boldsymbol{H}$, $\boldsymbol{S}$) denotes the thermodynamic function of H^+ in the standard state, and all other terms have their usual meaning. Using pK_1 = 1.252, $\Delta H^0(K_1)$ = 3.76 ± 0.42 kJ mol^{-1} ($\boldsymbol{I}$ = 0, 25^{o}C)[21], $\boldsymbol{X}^0(H^+)$ = 0 (by convention) the activation parameter data yield $\boldsymbol{G}(TS_2^{\neq})$ – $\boldsymbol{G}(TS_1^{\neq})$ = -12.8 ± 0.2 kJ mol^{-1}, $\boldsymbol{H}(TS_2^{\neq})$ – $\boldsymbol{H}(TS_1^{\neq})$ = 26.4 ± 9.3 kJ mol^{-1} and $\boldsymbol{S}(TS_2^{\neq})$–$\boldsymbol{S}(TS_1^{\neq})$ = + 130 ± 32 J K^{-1} mol^{-1} (25^{o}C). This reflects how the enthalpy and entropy factors control the stabilities of the transition states. In other words $TS_2^{\neq}$ in comparison to $TS_1^{\neq}$ is assembled with greater energy demand which is more than compensated by the entropy gain.

The intramolecular electron transfer for $Mn^{III}(salen)(OH_2)(OX)^-$($10^6k_4$ = 0.03 ± 14 at 35^{o}C) is virtually insignificant. The same is also true for the reaction: $Mn^{III}(salen)(OH_2)_2^+$ + H_2OX (k_3 =0.13 ± 0.47 dm^3 mol^{-1} s^{-1}, 35^{o}C, see Table 2). We attempted to examine the reactions via k_0 and k_3 paths using SDS as a probe. Our aim was to selectively partition the neutral H_2OX moiety along with $Mn^{III}(salen)(OH_2)_2^+$ and $Mn^{III}(salen)(OH_2)(HOX)$ into the anionic micellar pseudo phase and make these reaction paths feasible at a site (i.e. micelle layer) away from the bulk aqueous phase. Our results, however, did not reveal any partitioning of $Mn^{III}(salen)(OH_2)(HOX)$ and H_2OX into the anionic micelles at the experimental pH (= 3.9). Higher acidity could not be maintained to avoid the competitive pseudo phase ion-exchange equilibrium for $Mn^{III}(salen)(OH_2)_2^+{}_M/H^+{}_W$. However, it enabled us to assess the micellar binding of the diaqua complex via ion-exchange equilibrium. The calculated value of the equilibrium constant, K_{ex} (= 10.4 ± 0.8) is marginally higher than the same for the $Na^+{}_M/H^+{}_W$ exchange reported earlier (K_{ex} = 1, 2- 4)[39,40] and comparable to that of *trans*-$(OH_2)Co^{III}(SO_3)^+$ (K_{ex} = 10 for β = 0.6 at 25^{o}C).[41]

We undertook the study of the effect of azide ion (N_3^-) on the redox reaction as a probe for the reaction mechanism. Under the experimental conditions N_3^- is not a reductant like HOX^-. The value of the binding constant (Q_4) for N_3^- compares well with that of HOX^- (Q_1). The difference in the values of k_1 and k_8 (k_1/k_8 = 1.6 ± 0.3 at 40^{o}C) is not appreciable.

593 This further suggests that binding of N_3^- or HOX^- to Mn^{III} does not lead to any significant
594 difference in the rate of reduction by HOX^- that follows. Hence the study of the effect of N_3^-
595 validates the fact that *trans*-$(H_2O)Mn^{III}$(salen)(HOX) is kinetically stable to intramolecular
596 electron transfer, $HOX_{(bound)} \xrightarrow{e} Mn^{III}$.

597

598 ## 4. Conclusion

599 The electron transfer between *trans*-Mn^{III}(salen)$(OH_2)_2^+$ and oxalate species (H_2OX,
600 HOX^-, OX^{2-}) is preceded by fast and reversible aqua ligand substitution by HOX^- resulting
601 in *trans*-Mn^{III}(salen)(OH_2)(HOX). The activation parameters for the formation and
602 dissociation of the HOX complex are in support of associative interchange mechanism ($\boldsymbol{I}_a$).
603 The *trans*-Mn^{III}(salen)(OH_2)(HOX) and its conjugate base analogue, *trans*-
604 MnIII(salen)$(OH_2)(OX)^-$ are kinetically inert to intramolecular reduction of Mn^{III} centre by
605 the bound HOX^-/OX^{2-}; the former undergoes facile redox reaction with HOX^- and H_2OX
606 while the latter by only HOX^- under mild acidic condition ($2 \leq pH \leq 6$). Structure
607 optimization by DFT shows that there is a strong *structural trans* effect of OX^{2-} in *trans*-
608 Mn^{III}(salen)$(OH_2)(OX)^-$ (unlike for its conjugate acid form) resulting in complete expulsion
609 of H_2O from the Mn^{III} centre and resulting in a five coordinate species , Mn^{III}(salen)$(OX)^-$
610 with the H_2O molecule hydrogen bonded to the phenoxide moiety. The *trans*-
611 $(H_2O)Mn^{III}$(salen)(HOX), however, assumes a distorted octahedral structure with a long
612 Mn^{III}–OH_2 bond. It is possible for the *trans*-Mn^{III}(salen)(OH_2)(HOX) to add HOX/H_2OX
613 forming the *trans*-(HOX)Mn^{III}(salen)$(HOX/H_2OX)^{-/0}$ although such species are not accessible
614 under the experimental conditions. However, the computational study supports the possibility
615 of inner sphere electron transfer processes in the k_1 and k_2 paths. The computed structure of
616 *trans*-(HOX)Mn^{III}(salen)(H_2OX) with intramolecular hydrogen bond involving the bound

phenoxide and H_2OX, suggests that the intimate redox step in the k_2 path is essentially a proton controlled electron transfer process. The study of the effects of anionic micelles of SDS (sodium dodecyl sulphate) and azide ion provide further support in favor the proposed reaction paths.

Supplementary Material

Figures **S**1(a,b), S2, **S**3(a-d), S4(a,b), S5; Tables S1(a-c), S(2-8) are provided as Electronic Supplementary Information .

Acknowledgements

Financial support from the University grants Commission (UGC), New Delhi in terms of a Teacher Fellowship to AKK (Ref. T. F.OU3-007-1/10-11 (ERO)) is acknowledged. AKK thanks the Odisha Education Department and the authority of Sishu Ananta Mahavidyalaya, Khurda, Odisha, India for granting study leave. Authors are thankful to Prof. Gautam K Lahiri, Indian Institute of Technology, Mumbai for ESR measurement. HSB acknowledges DST-INSPIRE Faculty fellowship award (IFA11-CH-01) for the financial support.

References

1. Y. G. Abashkin and S. K. Burt, *J. Phys. Chem. B*, 2004, **108**, 2708-2711.
2. Y. G. Abashkin and S. K. Burt, *Inorg. Chem.*, 2005, **44**, 1425-1432.
3. V. Lanza and G. Vecchio, *J. Inorg. Biochem.*, 2009, **103**, 381-388.
4. Y. Noritake, N. Umezawa, N. Kato and T. Higuchi, *Inorg. Chem.*, 2013, **52**, 3653-3662.

5. S. Melov, J. Ravenscroft, S. Malik, M. S. Gill, D. W. Walker, P. E. Clayton, D. C. Wallace, B. Malfroy, S. R. Doctrow and G. J. Lithgow, *Science*, 2000, **289**, 1567-1569.

6. T. Katsuki, *Coord. Chem. Revs.*, 1995, **140**, 189-214.

7. M. Lakshmi Kantam and B. Bharathi, *Catal. Lett.*, 1998, **55**, 235-237.

8. M. Lakshmi Kantam, V. Neeraja, B. Bharathi and C. Venkat Reddy, *Catal. Lett.*, 1999, **62**, 67-69.

9. B. M. Choudary, M. L. Kantam, B. Bharathi and C. R. Venkat Reddy, *J. Molecular Catalysis A: Chemical*, 2001, **168**, 69-73.

10. S. Gangopadhyay, M. Ali and P. Banerjee, *Coord. Chem. Revs.*, 1994, **135–136**, 399-427.

11. J. P. McEvoy, J. A. Gascon, V. S. Batista and G. W. Brudvig, *Photochem. Photobiol. Sci.*, 2005, **4**, 940-949.

12. T. A. Betley, Y. Surendranath, M. V. Childress, G. E. Alliger, R. Fu, C. C. Cummins and D. G. Nocera, *Phil. Trans. R. Soc. B: Biological Sciences*, 2008, **363**, 1293-1303.

13. Derrick R. J. Kolling, N. Cox, Gennady M. Ananyev, Ron J. Pace and G. C. Dismukes, *Biophys. J.*, 2012, **103**, 313-322.

14. I. C. Kuan and M. Tien, *Proc. Natl. Acad. Sci. USA*, 1993, **90**, 1242-1246.

15. M. M. Whittaker, H.-Y. Pan, E. T. Yukl and J. W. Whittaker, *J. Biol. Chem.*, 2007, **282**, 7011-7023.

16. A. C. Dash and A. Das, *Int. J. Chem. Kinet.*, 1999, **31**, 627-635.

17. A. Kar, A. Acharya, G. Pradhan and A. C. Dash, *J. Chem. Sci.*, 2014, **126**, 547-559.

18. T. J. Jones and R. M. Noyes, *J. Phys. Chem.*, 1983, **87**, 4686-4689.

19. S. Mukhopadhyay, S. Chaudhuri, R. Das and R. Banerjee, *Can. J. Chem.*, 1993, **71**, 2155-2159.

20. H. M. Irving, M. G. Miles and L. D. Pettit, *Anal. Chim. Acta.*, 1967, **38**, 475-488.

21. A. E. Martell and R. M. Smith, in *Critical Stability Constants*, eds. A. E. Martell and R. M. Smith, Plenum Press, New York, 1977, vol. 3, p. 92.

22. A. Panja, N. Shaikh, M. Ali, P. Vojtíšek and P. Banerjee, *Polyhedron*, 2003, **22**, 1191-1198.

23. S. Nayak and A. C. Dash, *Transition Met. Chem.*, 2006, **31**, 316-324.

24. K. Kovacs, B. Vizvari, M. Riedel and J. Toth, *Phys. Chem. Chem. Phys.*, 2004, **6**, 1236-1242.

25. R. H. Ottewill, in *Surfactants*, ed. T. F. Tadros, Academic Press, London, 1984, pp. 8, Table-1.

26. S. Nayak and A. C. Dash, *Ind. J. Chem. Sec. A*, 2003, **42A**, 2427-2438.

27. R. Ahlrichs, M. Bär, M. Häser, H. Horn and C. Kölmel, *Chem. Phys. Lett.*, 1989, **162**, 165-169.

28. O. Treutler and R. Ahlrichs, *J. Chem. Phys.*, 1995, **102**, 346-354.

29. O. Vahtras, J. Almlöf and M. W. Feyereisen, *Chem. Phys. Lett.*, 1993, **213**, 514-518.

30. K. Eichkorn, O. Treutler, H. Öhm, M. Häser and R. Ahlrichs, *Chem. Phys. Lett.*, 1995, **242**, 652-660.

31. K. Eichkorn, O. Treutler, H. Öhm, M. Häser and R. Ahlrichs, *Chem. Phys. Lett.*, 1995, **240**, 283-290.

32. C. F. Macrae, I. J. Bruno, J. A. Chisholm, P. R. Edgington, P. McCabe, E. Pidcock, L. Rodriguez-Monge, R. Taylor, J. van de Streek and P. A. Wood, *J. Appl. Cryst.*, 2008, **41**, 466-470.

33. I. Salem and A. Gemeay, *Transit. Met. Chem.*, 1996, **21**, 130-134.

34. J. J. Morgan in *Metals in Biological Systems*, eds. A. Sigel and H. Sigel, Marcel Dekkewr Inc., New York, 2000, vol 37, pp7, Table 2.

35. D. Lieb, A. Zahl, T. E. Shubina and I. Ivanovic-Burmazovic, *J. Am. Chem. Soc.*, 2010,**132**, 7282-7284

36. M. A. Suwyn and R. E. Hamm, *Inorg. Chem.*, 1967, **6**, 2150-2154.

37. A. C. Dash and R. K. Nanda, *Inorg. Chem.*, 1974, **13**, 655-661.

38. G. B. Wijeratne, B. Corzine, V. W. Day and T. A. Jackson, *Inorg. Chem.*, 2014, **53**, 7622-7634.

39. L. H. Romsted, in *Surfactants in Solutions*, eds. K. L. Mittal and B. Lindman, Plenum, New York, 1984, vol. 2, pp. 1038, Table 1 (foot note *a*).

40. C. J. Garnett, A. J. Lambie, W. H. Beck and M. Liler, *J. Chem.. Soc. Faraday Trans. 1*, 1983, **79**, 953-964.

41. A. C. Dash and S. S. Mohammed, *Ind. J. Chem. Sec. A*, 1991, **30A**, 653-659.

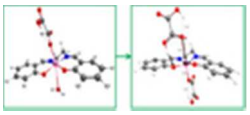

5x2mm (600 x 600 DPI)

A table of Contents entry

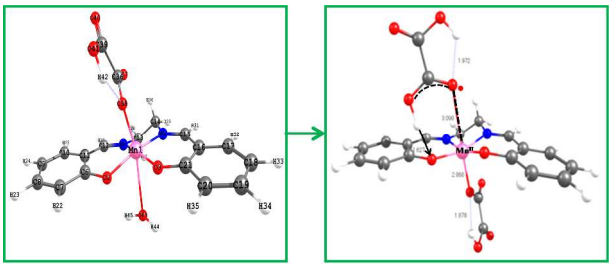

$Mn^{III}(salen)(OH_2)_2^+$ undergoes reversible anation by HOX^- via $\boldsymbol{I}_a$ mechanism followed by proton controlled electron transfer involving $Mn^{III}(salen)(HOX)$ and H_2OX.